

Western  Graduate&PostdoctoralStudies

Western University
Scholarship@Western

Electronic Thesis and Dissertation Repository

8-21-2012 12:00 AM

The Distribution and Functional Properties of PMLD-Linked CX47 Mutations on CX47/CX47 Homotypic and CX47/CX43 Heterotypic Gap Junctions

Mi Seong Kim
The University of Western Ontario

Supervisor
Dr. Donglin Bai
The University of Western Ontario

Graduate Program in Physiology
A thesis submitted in partial fulfillment of the requirements for the degree in Master of Science
© Mi Seong Kim 2012

Follow this and additional works at: <https://ir.lib.uwo.ca/etd>



Part of the [Cellular and Molecular Physiology Commons](#)

Recommended Citation

Kim, Mi Seong, "The Distribution and Functional Properties of PMLD-Linked CX47 Mutations on CX47/CX47 Homotypic and CX47/CX43 Heterotypic Gap Junctions" (2012). *Electronic Thesis and Dissertation Repository*. 737.

<https://ir.lib.uwo.ca/etd/737>

This Dissertation/Thesis is brought to you for free and open access by Scholarship@Western. It has been accepted for inclusion in Electronic Thesis and Dissertation Repository by an authorized administrator of Scholarship@Western. For more information, please contact wlsadmin@uwo.ca.

**THE DISTRIBUTION AND FUNCTIONAL PROPERTIES OF PMLD-LINKED
CX47 MUTATIONS ON CX47/CX47 HOMOTYPIC AND CX47/CX43
HETEROTYPIC GAP JUNCTIONS**

(Spine Title: Characterization of PMLD-linked Cx47 mutants)

(Thesis format: Monograph)

By

Mi Seong Kim

Graduate Program in Physiology

A thesis submitted in partial fulfillment
Of the requirements for the degree of
Master of Science

The School of Graduate and Postdoctoral Studies
The University of Western Ontario
London, Ontario, Canada

© Mi Seong Kim 2012

THE UNIVERSITY OF WESTERN ONTARIO
SCHOOL OF GRADUATE AND POSTDOCTORAL STUDIES

CERTIFICATE OF EXAMINATION

Supervisor

Dr. Donglin Bai

Supervisory Committee

Dr. Gerald Kidder

Dr. Wei-Yang Lu

Dr. L. Stan Leung

Examiners

Dr. Dale Laird

Dr. Stephen Sims

Dr. Arthur Brown

The thesis by

Mi Seong Kim

entitled:

THE DISTRIBUTION AND FUNCTIONAL PROPERTIES OF PMLD-LINKED CX47
MUTATIONS ON CX47/CX47 HOMOTYPIC AND CX47/CX43 HETEROTYPIC GAP
JUNCTIONS

is accepted in partial fulfilment of the
requirements for the degree of
Master of Science

Date _____

Chair of the Thesis Examination Board

Abstract

Gap junctions (GJ) allow direct intercellular communication, and consist of connexins (Cx). In the mammalian central nervous system, oligodendrocytes express Cx29, Cx32 and Cx47, whereas astrocytes express Cx26, Cx30 and Cx43. Cx47/Cx47 GJs couple oligodendrocytes, and Cx47/Cx43 channels are the primary heterotypic GJs at oligodendrocyte/astrocyte junctions. Interestingly, mutations in Cx47 have been linked to central hypomyelinating Pelizaeus Merzbacher-like Disease (PMLD). My aim is to determine the cellular distribution and functional properties of PMLD-associated Cx47 mutants (I46M, G149S, G236R, G236S, M286T, T398I). All mutants were detected at the cell-cell interface. These mutants, except G149S and T398I, showed no electrical coupling in both Cx47/Cx47 and Cx47/Cx43 GJ channels. G149S and T398I formed homotypic and heterotypic channels of apparently normal functions. These results suggest that the tested Cx47 mutants, except G149S and T398I, lead to PMLD likely due to disruption in Cx47/Cx47 and/or Cx47/Cx43 GJ functions in the macroglial network.

Keywords: gap junctions, connexins, hypomyelination, Pelizaeus Merzbacher-like disease, connexin47

Dedication

I would like to dedicate my thesis
to my beloved mom and dad.

Acknowledgments

I would like to thank, first and foremost, my supervisor Dr. Donglin Bai for the opportunity to expand my knowledge in science. His assistance and guidance along with his vast knowledge of electrophysiology and encouragement allowed me to gain invaluable experience in scientific research. I am also grateful to all my committee members, Drs. Gerald Kidder, Stan Leung and Wei-Yang Lu, for all the precious advice and support. I would like to express my appreciation towards the Bai laboratory, especially Drs. Xiang-Qun Gong and Yiguo Sun and Li Xin for all the help and advice for laboratory techniques and technical support. I could not have finished my project without your hands-on advice. It has been a great pleasure to work with you all. Lastly, I thank all my family and friends for unconditional support and patience. Thank you for being so understanding and supportive, and for never ending motivations.

Table of Contents

	Page
CERTIFICATE OF EXAMINATION	ii
ABSTRACT.....	iii
DEDICATION.....	iv
ACKNOWLEDGMENTS	v
TABLE OF CONTENTS.....	vi
LIST OF FIGURES	viii
LIST OF TABLES.....	ix
LIST OF ABBREVIATIONS AND NOMENCLATURE.....	x
CHAPTER 1. Introduction.....	1
1.1. Gap junctions.....	2
1.2. Connexins	4
1.3. Gap junction configuration.....	4
1.4. Oligomerization of Cxs	7
1.5. Docking compatibility between two connexons.....	7
1.6. Transjunctional Voltage-dependent gating of gap junction channels	8
1.7. Connexins in macroglia.....	10
1.8. Oligodendrocyte-to-astrocyte coupling.....	12
1.9. Oligodendrocyte-to-oligodendrocyte coupling.....	13
1.10. Macroglial connexins and myelination in the CNS	14
1.11. Connexin47 and Pelizaeus Merzbacher-like Disease.....	15
1.12. Hypothesis and objectives.....	18
CHAPTER 2. Methods	19
2.1. Connexin47 and the mutant cDNA construct generation.....	20
2.2. Connexin43 cDNA construct generation.....	23
2.3. Cell culture and transfection.....	25
2.4. Fixation and fluorescent imaging	26
2.5. Electrophysiological recordings	26

2.6. Statistical analysis	29
CHAPTER 3. Results.....	30
3.1. Fluorescent imaging and Vj-gating analysis of Cx47 homotypic GJs	31
3.2. Fluorecent imaging of Cx47 mutant homotypic pairs.	36
3.3. Conductance measurements of Cx47 mutant homotypic GJs.	38
3.4. Vj-gating analysis of functional Cx47 mutant homotypic GJs.....	40
3.5. Fluorescent imaging of Cx47 and Cx47 mutant heterotypic pairs with Cx43. ...	42
3.6. Vj-gating of Cx47/Cx43 heterotypic channels.	44
3.7. Conductance measurements of Cx47 mutant heterotypic channels with Cx43...	47
3.8. Vj-gating properties of functional Cx47 mutant/Cx43 heterotypic GJs.....	49
CHAPTER 4. Discussion.....	51
4.1. Overall study.....	52
4.2. Localization of Cx47-GFP at the cell-cell interface	55
4.3. Homotypic Cx47-GFP gap junction channels and PMLD mutants	56
4.4. Co-localization of Cx47-GFP and Cx43-mRFP at the cell-cell interface	59
4.5. Heterotypic Cx47-GFP/Cx43-mRFP gap junction channels and PMLD mutants.....	60
4.6. PMLD-linked Cx47 mutants and hemichannel functions	63
4.7. Clinical phenotypes of Cx47 mutants.....	64
4.8. Cx47 is the critical Cx that constitutes oligodendrocyte-to-oligodendrocyte GJs.	65
4.9. Cx47 is critical for O/A coupling.	67
4.10. Conclusion.....	68
REFERENCES	69
CURRICULUM VITAE.....	74

List of Figures

1-1	Schematic diagram of a gap junction channel and connexin topology	3
1-2	Configuration of gap junction channels	6
1-3	Gap junctions in oligodendrocyte and astrocyte networks	11
1-4	Cx47 topology and mutant map	17
2-1	Human Cx47-GFP topology and mutant map	22
2-2	Human Cx43-mRFP topology	24
2-3	Dual whole-cell patch clamp	28
3-1	The localization and macroscopic V_j -gating properties of Cx47-GFP homotypic gap junctions	33
3-2	Localization of Cx47 mutants in HeLa cells	37
3-3	Junctional conductance (G_j) measurements of Cx47 mutant homotypic channels	39
3-4	V_j -gating properties of G149S and T398I homotypic gap junctions	41
3-5	Co-localization of Cx47 (or Cx47 ^{G149S}) and Cx43-mRFP at cell-cell interfaces in HeLa cell pairs	43
3-6	V_j -gating properties of Cx47/Cx43 heterotypic gap junctions	45
3-7	Junctional conductance (G_j) measurements of Cx47 mutant heterotypic channels with Cx43.	48
3-8	V_j -gating properties of Cx47 mutant/Cx43 heterotypic gap junctions	50

List of Tables

2-1	Primers used to generate Cx47 mutants	21
3-1	Boltzmann parameters of Cx47/Cx47 and Cx47/Cx43 channels	35
4-1	Summary of localization and functional status of Cx47 mutants	54

List of abbreviations and nomenclature

A	astrocyte
A	steepness of voltage sensitivity
CMTX	Charcot-Marie-Tooth syndrome
CNS	central nervous system
CT	carboxyl terminus
Cx	connexin
DAPI	4',6-diamidino-2-phenylindole
DMEM	Dulbecco's modified eagle medium
E1	first extracellular loop
E2	second extracellular loop
ER	endoplasmic reticulum
GFP	green fluorescent protein
GJ	gap junction
G_j	macroscopic junctional conductance
$G_{j,ss}$	steady-state conductance normalized to the corresponding peak G_j
GJIC	gap junctional intercellular communication
G_{max}	the maximum normalized steady-state conductance
G_{min}	the minimum normalized steady-state conductance
HeLa	cervical cancer cell line
I_j	junctional current
IL	intracellular loop
IRES	internal ribosome entry site

kDa	kilo-dalton
mRFP	monomeric red fluorescent protein
MRI	magnetic resonance imaging
N2A	neuroblastoma cells
NT	amino terminus
O	oligodendrocyte
O/A	oligodendrocyte/astrocyte
O/O	oligodendrocyte/oligodendrocyte
ODDD	oculodentodigital dysplasia
PMLD	Pelizaeus Merzbacher-like disease
RFP	red fluorescent protein
SEM	standard error of mean
TM	transmembrane domain
V_j	transjunctional voltage
V_j-gating	transjunctional voltage-dependent gating
V_o	the voltage at which the normalized steady-state conductance is half maximal
WT	wild-type
ZO-1	zonula occludens-1

1. Introduction

1.1. Gap junctions

Gap junctions (GJ) are ubiquitous clusters of intercellular channels formed between neighbouring cells. Each gap junction channel is formed by two end-to-end docked hemichannels, also known as connexons, which themselves consists of six connexin subunits (Cx) (Fig 1-1). These intercellular channels provide a direct conduit for movement of ions and small molecules (< 1 kDa) including metabolites and secondary messengers, mediating gap junctional intercellular communication (GJIC) (Sohl and Willecke, 2004). GJIC is crucially involved in many biological processes including development, differentiation and neuronal activity (Goodenough and Paul, 2009). Mutations in Cxs have been linked to many human diseases such as Pelizaeus Merzbacher-like disease (PMLD; Cx47) (Henneke et al., 2008), oculodentodigital dysplasia (ODDD; Cx43) (Paznekas et al., 2003), Charcot-Marie-Tooth syndrome (CMTX; Cx32) (Hanemann et al., 2003), deafness (Cx26, Cx30) (Al-Achkar et al., 2011; Wang et al., 2011) and cataracts (Cx50, Cx46) (Arora et al., 2008; Wang and Zhu, 2012). Various experimental approaches using fluorescent dye transfer assays, electrophysiological recordings and Cx gene knock-out mice models provide tools to study GJ channel functions including dye and ionic permeability, transjunctional voltage-dependent gating (V_j -gating) and *in vivo* phenotypes (Goodenough and Paul, 2009; Sohl and Willecke, 2004).

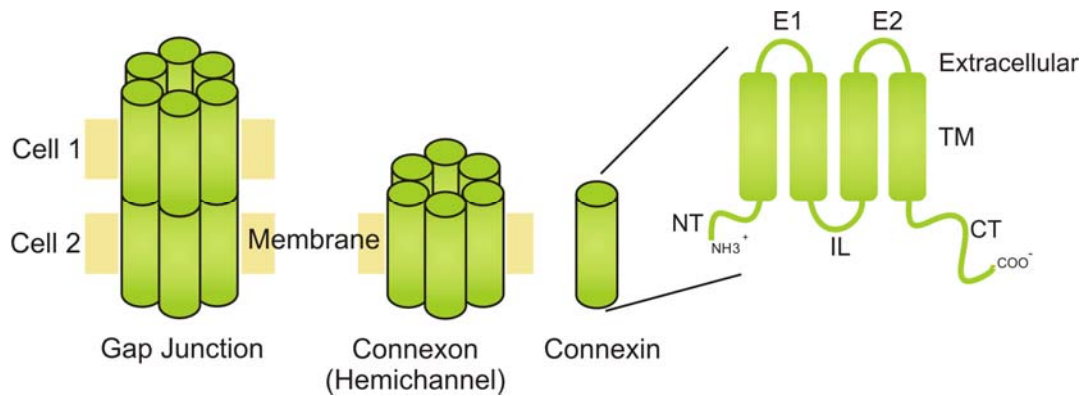


Figure 1-1. Schematic diagram of a gap junction channel and connexin topology. Gap junctions are composed of two hexameric hemichannels called connexons, and each connexon, in turn, is made up of six connexin (Cx) proteins. All Cxs share a common structural topology of four transmembrane domains (TM1-TM4), intracellular amino- (NT) and carboxyl- (CT) termini, one intracellular loop (IL) and two extracellular loops (E1 and E2).

1.2. Connexins

Connexins (Cxs), the basic subunits of gap junctions, comprise a family of highly conserved integral membrane proteins. Currently, 20 Cx genes in the mouse and 21 Cx genes in the human genome have been identified, where each Cx is designated according to its theoretical molecular mass in kDa. The Cx isoforms possess a common structural topology of four transmembrane domains, two extracellular loops, one intracellular loop and cytoplasmic amino- and carboxyl- termini (Fig 1-1;(Goodenough and Paul, 2009; Sohl and Willecke, 2004). Among various Cxs, the transmembrane domains, amino terminus and the two extracellular loops show the most conserved sequences. On the contrary, the intracellular loop and the carboxyl terminus vary in length and sequence (Kovacs et al., 2007). Furthermore, each connexin shows a unique distribution pattern among various cell types. These differences among various Cxs in both structure and distribution result in the formation of gap junctions with diverse configurations and functions (Orthmann-Murphy et al., 2008; Sohl and Willecke, 2004).

1.3. Gap junction configuration

In mammalian cells, it is often found that more than one type of Cx are co-expressed within the same cell. Therefore, six identical or different connexins may oligomerize, forming a homomeric or heteromeric connexon, respectively (Fig 1-2). The connexon or hemichannel may then dock with the same or different connexon from an apposing cell, and make up a homotypic or heterotypic gap junction channel, respectively (Fig. 1-2). When a complete GJ channel is formed, each GJ

channel possesses unique functional characteristics of dye permeability, single channel conductance and V_j -gating, depending on the component Cxs (Sohl and Willecke, 2004; White et al., 1994).

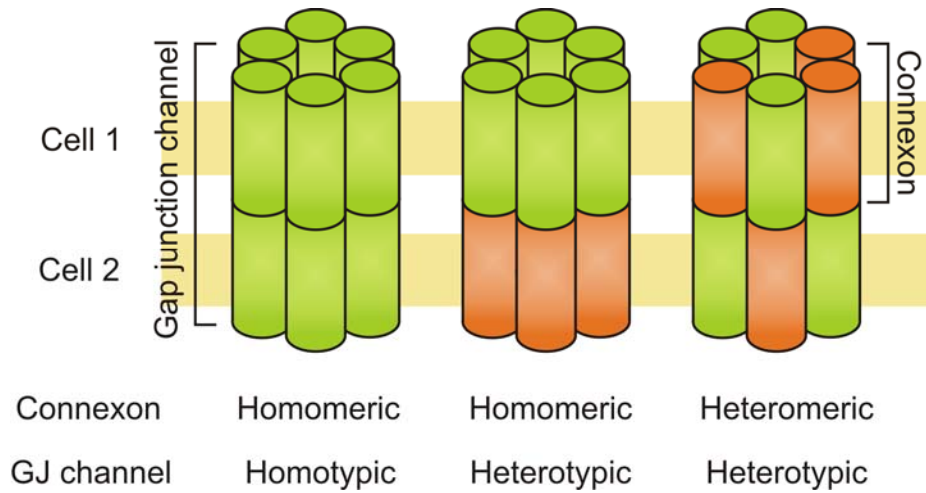


Figure 1-2. Configuration of gap junction channels. A homomeric connexon is composed of six identical Cxs, whereas a heteromeric connexon consists of two or more different Cxs. When the same connexons dock together, they form homotypic gap junction channels, whereas different connexons dock together to form heterotypic gap junction channels.

1.4. Oligomerization of Cxs

As described above, six Cxs oligomerize together to form a connexon (also referred to as hemichannel). In this oligomerization process, each Cx has a distinct location in which Cxs oligomerize into connexons or hemichannels. For example, Cx43 oligomerizes in the trans-Golgi network, whereas Cx32 oligomerization occurs in the endoplasmic reticulum (ER) (Das Sarma et al., 2002; Musil and Goodenough, 1993). More interestingly, Cxs show distinct compatibility in oligomerization with other Cxs to form a connexon. For example, Cx43 can form heteromeric connexons with Cx45 but not with Cx26 (Gemel et al., 2004; Martinez et al., 2002). Furthermore, a recent study using chimeras where a domain(s) of Cx43 was exchanged with the corresponding domain(s) of Cx26 revealed that TM3 is critical for Cx43 oligomerization, but not for Cx26 oligomerization, suggesting that each Cx has distinct domains that determine the Cx oligomerization compatibility (Martinez et al., 2011). As cells may express more than one Cx, it is possible that both homomeric and heteromeric connexons are formed. However, for the purpose of this study, I focused on homomeric connexons.

1.5. Docking compatibility between two connexons

In the formation of GJ channels, Cx proteins show selective interaction with other Cx proteins in docking of two connexons to form functional heterotypic channels. Electrophysiological recordings on *Xenopus* oocytes showed that Cxs that successfully formed functional homotypic channels did not always form functional heterotypic channels when paired with different Cxs (White et al., 1994). For

example, Cx43 can form functional heterotypic channels with Cx46 but not with Cx50 (White et al., 1994). More interestingly, Cxs established heterotypic channel properties different from their homotypic channel characteristics. For example, Cx26/Cx32 channels showed intermediate dye permeability between the two homotypic channels (Cao et al., 1998). Heterotypic Cx46/Cx50 channels established symmetric transjunctional voltage-dependent response despite the distinct properties of their homotypic channels (White et al., 1994). In addition, this study suggested that E2 is likely to be the determinant of the docking selectivity through chimera approaches (Nakagawa et al., 2011; White et al., 1994). This view was further supported by the atomic structure of human Cx26 (hCx26) and mutagenesis (Nakagawa et al., 2011). Overall, the Cx compatibility in docking determines the functional gap junctional interaction between cells, and ultimately dictates the contribution of Cxs in maintaining organ homeostasis.

1.6. Transjunctional Voltage-dependent gating (V_j -gating) of gap junction channels

“Gating” refers to the molecular transitions of channels between open and closed states, which physically allows or restricts ionic or non-ionic conductive pathway. GJ channels undergo the gating in response to transjunctional voltage (V_j), cytoplasmic acidification, change in intracellular Ca^{2+} concentration, and chemical uncouplers (Bukauskas and Verselis, 2004).

GJ channel gating is influenced by two types of electrical field: the voltage difference between the two cell cytoplasms (transjunctional voltage; V_j); and the voltage difference between the cell interior and the extracellular medium (V_m). The

conductance of many gap junctions is only sensitive to V_j , while others show both V_j - and V_m -dependence. V_j is established when the membrane voltages in two cells of a pair are not equal. In V_j -gating process, it is commonly found that the steady-state junctional conductance (G_j) reaches residual conductance ranging from ~5% to 40% of the maximum G_j , depending on the Cx isoforms (Bukauskas and Verselis, 2004).

Single channel recordings demonstrated that GJ channels possess two distinct V_j -gating processes that mediate transitions between different conductance states. Transitions between the open state and residual states are usually fast (<1-2 ms) and known as “fast” V_j -gating; transitions between the residual state and closed state take tens of milliseconds and are termed “slow” V_j -gating (Bukauskas and Verselis, 2004).

Previously, structure modelling of hCx26 and the mutations at the M1/E1 boundary affect voltage sensing, suggesting that these domains may play a role as a V_j sensor (Maeda et al., 2009; Verselis et al., 1994). When enhanced green fluorescent protein (EGFP) was fused to the CT tail of Cx43, the gap junction channel lost transitions to the residual state (fast V_j gating). However, V_j gating properties of mouse Cx47-EGFP channels were indistinguishable from the untagged wild-type Cx47 channels, suggesting that the involvement of the CT domain in fast V_j gating may be Cx specific (Bukauskas et al., 2001; Teubner et al., 2001).

1.7. Connexins in macroglia

The mammalian central nervous system (CNS) contains two major macroglial cells, oligodendrocytes and astrocytes. Oligodendrocytes are responsible for myelination of axons to promote rapid saltatory conduction of action potentials (Kamasawa et al., 2005). Astrocytes support neuronal activities including modulation of synaptic transmission, neuronal synchronization and regulation of cerebral blood flow (Volterra and Meldolesi, 2005). These two types of macroglial cells are known to express distinct sets of Cxs, and form extensive gap junction couplings among themselves and between these two macroglial cell types (Maglione et al., 2010; Orthmann-Murphy et al., 2008). Oligodendrocytes express Cx29, Cx32 and Cx47, while astrocytes express Cx26, Cx30 and Cx43 (Fig 1-3; (Altevogt et al., 2002; Kleopa et al., 2004; Kunzelmann et al., 1999; Menichella et al., 2003; Yamamoto et al., 1990). Together, these Cxs may form homomeric or heteromeric hemichannels. The hemichannels then may dock with the same or different hemichannels to form GJ channels that mediate propagation of Ca^{2+} waves between astrocytes, and buffering of K^+ released during neuronal activity by oligodendrocytes and astrocytes (Kamasawa et al., 2005; Menichella et al., 2006; Scemes and Giaume, 2006).

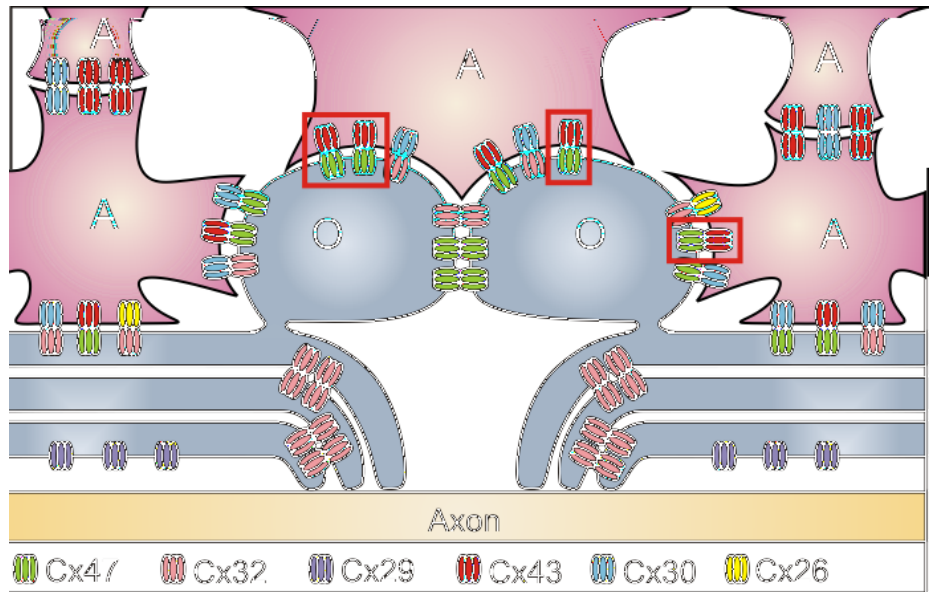


Figure 1-3. Gap junctions in oligodendrocyte and astrocyte networks.

Astrocytes form Cx43/Cx43 or Cx30/Cx30 homotypic GJs. Oligodendrocytes are coupled to astrocytes via Cx47/Cx43 (shown in red boxes), Cx32/Cx30, Cx47/Cx30 and Cx32/Cx26 heterotypic channels. Oligodendrocytes were found to be coupled to each other via GJs made with Cx47 and/or Cx32. Cx32 in oligodendrocytes is also known to form homotypic reflexive gap junctions. Cx29 does not form gap junctions, but may form hemichannels at adaxonal membranes (Altevogt et al., 2002; Kleopa et al., 2004).

1.8. Oligodendrocyte-to-astrocyte coupling

In the CNS, astrocytes are known to form homotypic gap junctions among themselves, but oligodendrocytes were believed to be coupled to each other only through astrocyte mediators (Rash et al., 2001). At these oligodendrocyte-astrocyte (O/A) junctions, oligodendrocytes and astrocytes form extensive heterotypic gap junction networks as the two cells express different Cx sets (Fig 1-3).

Previously, immunolabeling and electrophysiological recordings on gap junction-deficient model cells transfected with these glial Cxs, indicated that Cx47/Cx43 and Cx32/Cx30 could dock and form functional heterotypic channels, while Cx47/Cx30 and Cx32/Cx43 did not (Orthmann-Murphy et al., 2007b). Triple immunolabeling on mouse spinal cord showed co-localization of Cx47 with Cx30 and Cx43, and Cx32 with Cx26 (Altevogt and Paul, 2004). In another study, immunolabeling on mouse brain in Cx32-deficient mice indicated reduction of Cx30 and Cx26, and abundant co-localization of Cx47 with Cx43 at O/A junctions (Nagy et al., 2003). Further, a dye transfer study using neurobiotin demonstrated functional Cx47/Cx43, Cx47/Cx30, Cx32/Cx30 and Cx32/Cx26 heterotypic channels in HeLa cells and primary astrocyte cultures (Magnotti et al., 2011).

Although different experimental approaches provided different perspectives on heterotypic gap junction channels at O/A junctions, Cx47/Cx43 and Cx32/Cx30 channels are widely known to be the main ones. However, the abundance of Cx47 over Cx32 between oligodendrocyte somata and astrocytic processes, according to immunocytochemistry and freeze-fracture replica immunogold labelling, suggest the dominant expression of Cx47/Cx43 channels over Cx32/Cx30 channels

(Kamasawa et al., 2005; Nagy et al., 2003). Also, unlike in Cx47-null mice, no evident difference in O/A coupling in the neocortex of Cx32-null mice was observed, suggesting the functional importance of Cx47/Cx43 heterotypic GJ channels (Wasseff and Scherer, 2011). The cellular localization combined with the Cx knock-out studies suggests that Cx47/Cx43 heterotypic GJs are the primary GJs for O/A coupling.

1.9. Oligodendrocyte-to-oligodendrocyte coupling

Previously, oligodendrocytes were thought to form gap junctions only with astrocytes. However, recent dye coupling studies on mouse corpus callosum revealed that oligodendrocytes are also directly coupled to each other (Maglione et al., 2010; Wasseff and Scherer, 2011). Oligodendrocyte-to-oligodendrocyte (O/O) coupling was abolished in oligodendrocyte Cx47- and Cx47/Cx32-double- deficient mice, indicating that Cx47 GJs are the key GJs for O/O GJIC. As predicted, when oligodendrocyte Cx32, astrocyte Cx43 or both Cx43 and Cx30 were knocked out, O/O coupling was still present, proposing functional importance for Cx47 in O/O GJ networks (Maglione et al., 2010). In another study, O/O coupling was more affected in mice lacking Cx32, compared to those lacking Cx47, suggesting that Cx32 plays a more essential role in O/O coupling in the neocortex (Wasseff and Scherer, 2011). These studies provided functional support for O/O coupling and demonstrated that Cx47 is the dominant contributor to the O/O coupling in these specific brain areas.

1.10. Macroglial connexins and myelination in the CNS

Connexins expressed in oligodendrocytes and astrocytes have been associated with central myelination. In Cx47 knock-out mice, no obvious phenotypic abnormalities were observed. Although demyelination was not detected in the spinal cords, electron microscopic analysis revealed conspicuous vacuolation of myelin in the optic nerve (Menichella et al., 2003; Odermatt et al., 2003). In contrast, Cx32 knock-out mice showed no myelin abnormalities in the CNS (Scherer et al., 1998). When both Cx47 and Cx32 were knocked out, the mice developed action tremor and tonic seizures, and eventually died around 6-8 postnatal weeks. In these mice, thinning and more abundant vacuolation in myelin sheaths and oligodendrocyte cell death were observed in the optic nerve (Menichella et al., 2003; Odermatt et al., 2003). Together, these phenotypes of oligodendrocyte Cx47- and Cx47/Cx32 double- knockout mice models postulate the importance of Cx47-mediated GJIC in maintaining normal myelination in the CNS.

Moreover, mutations in Cx47 or Cx43 were reported to cause hypomyelination in the CNS in humans. Mutations in the gene encoding Cx47 cause Pelizaeus-Merzbacher-like disease (PMLD) and hereditary spastic paraplegia (HSP) (Bugiani et al., 2006; Orthmann-Murphy et al., 2009). PMLD is a devastating dysmyelinating disease that results in nystagmus, impaired motor development and hypomyelination on magnetic resonance imaging (MRI) (Bugiani et al., 2006; Henneke et al., 2008; Salviati et al., 2007; Uhlenberg et al., 2004; Wang et al., 2010). Hereditary spastic paraplegia (HSP) is another hypomyelinating disease due

to mutations in Cx47, whose phenotypes are milder than those of PMLD (Orthmann-Murphy, et al., 2009). Surprisingly, some mutations in Cx43 result in oculodentodigital dysplasia (ODDD) that is also associated with CNS abnormalities including hypomyelination identified with MRI (Loddenkemper et al., 2002; Paznekas et al., 2003; Paznekas et al., 2009). These disease-linked mutations in Cx47 or Cx43 and associated clinical symptoms suggest that these mutations likely affect proper functions of oligodendrocytes by interrupting Cx47/Cx47 and/or Cx47/Cx43 GJs at the O/O and/or O/A junctions, respectively.

1.11. Connexin47 and Pelizaeus Merzbacher-like Disease

Currently, twenty-four different Cx47 mutations have been identified from PMLD and HSP patients (Fig 1-4; (Biancheri et al., 2012; Bugiani et al., 2006; Diekmann et al., 2010; Henneke et al., 2008; Orthmann-Murphy et al., 2007a; Orthmann-Murphy et al., 2009; Salviati et al., 2007; Sartori et al., 2008; Uhlenberg et al., 2004; Wang et al., 2010). When PMLD-linked Cx47 mutants were examined for localization, the wildtype (WT) and some mutants (M286T, G149S, T398I) were observed at the cell-cell junctions. However, some other mutant proteins (P90S, Y272D, A98G_V99insT and T265A) showed defects in trafficking and failed to reach the cell surface and cell-cell junctions to form GJ plaque-like structures (Diekmann et al., 2010; Orthmann-Murphy et al., 2007a). In functional studies, dual patch clamp recordings revealed that mutants P90S, Y272D and M286T did not form functional homotypic and heterotypic GJ channels with Cx43 regardless of their localization at the cell-cell interface (Orthmann-Murphy et al.,

2007a; Orthmann-Murphy et al., 2007b). The I36M mutation that caused milder phenotypes than PMLD mutants, formed GJ plaque-like structures but still failed to form functional homotypic and heterotypic channels with WT Cx43 (Orthmann-Murphy et al., 2009).

Previous studies showed that Cx47 mutants result in loss-of-function in their GJ channels or dysfunction in hemichannels (Diekmann et al., 2010; Orthmann-Murphy et al., 2007a; Orthmann-Murphy et al., 2009). Currently, the exact molecular mechanisms leading to the disease states are not clear. Furthermore, it still remains elusive as to the ability of some PMLD-linked Cx47 mutants to form functional homotypic Cx47/Cx47 and heterotypic Cx47/Cx43 GJs which constitute the primary GJs at O/O and O/A junctions, respectively. Here, as marked in Fig. 1-4, six PMLD-linked Cx47 mutations (I46M, G149S, G236R, G236S, M286T and T398I) from different domains that are already known to traffic to the cell-cell junctions or have not been studied, were selected. I attempted to elucidate the effects of these mutations on their capability of forming Cx47/Cx47 and/or Cx47/Cx43 GJ channels by investigating their cellular localization and electrical couplings in gap junction-deficient HeLa and mouse neuroblastoma (N2A) cell lines, respectively. This study would assist us in understanding the fundamental roles of Cx47-involving GJs in maintaining proper myelination in the CNS.

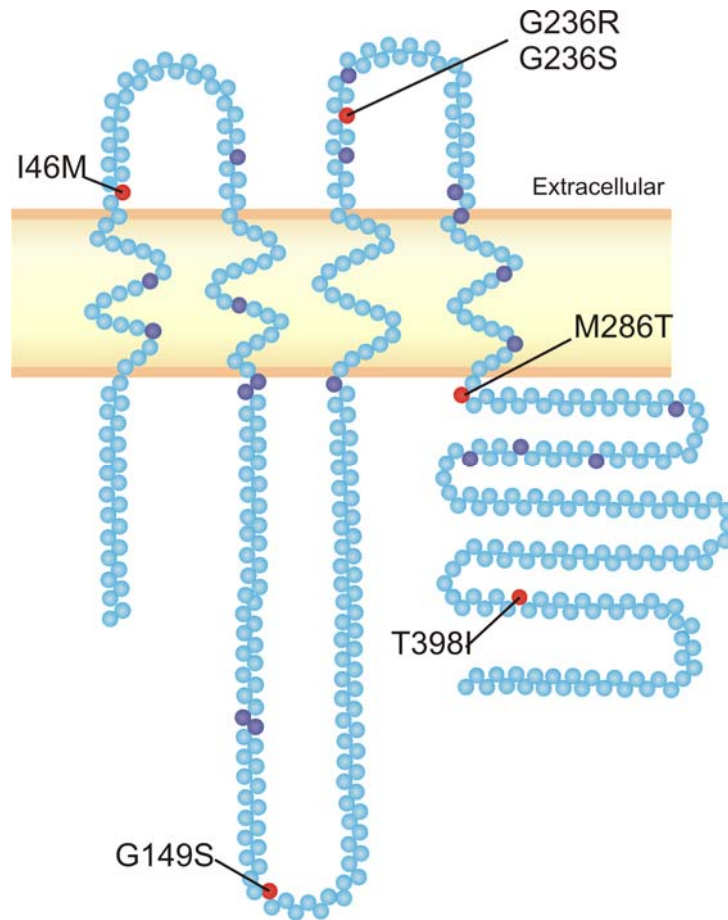


Figure 1-4. Cx47 topology and mutant map. Twenty-four mutations (red and purple) were reported from PMLD and HSP patients. The six mutants (red) were selected to be analyzed in this study.

1.12. Hypothesis and objectives

1) Hypothesis

Mutations in Cx47 that are associated with PMLD affect the homotypic Cx47/Cx47 and/or heterotypic Cx47/Cx43 gap junction channel functions through impaired localization to the membrane, formation of functional channels, and/or altered channel properties such as macroscopic junctional conductance and V_j -gating.

2) Objectives

- I. To determine whether Cx47 mutants are able to localize at cell-cell junctions, which is a pre-requisite for the formation of functional GJ channels.
- II. To determine whether Cx47 mutants can form functional homotypic GJ channels by themselves and/or heterotypic GJ channels with Cx43
- III. To determine if the V_j -gating properties of mutant homotypic and/or heterotypic Cx47mutant/Cx43 channels are modified.

2. Methods

2.1. **Conneixn47 and the mutant cDNA construct generation**

To generate a fusion construct of Cx47 with green fluorescent protein (GFP) tagged at the C-terminus, Cx47 cDNA was amplified by polymerase chain reaction (PCR) with the forward primer 5'-CTGGAATTCTTCTGGCCTGGAGAAGGAC-3' and the reverse primer 5'-CTGGTACCCAGCTCGCAAGCCAGCGCCCTCCGATCCACACGGTGGTCTT C-3'. The PCR product was subcloned into the pEGFP-N1 vector using EcoRI and KpnI restriction sites (Norclone Biotech Labs, London, ON). The plasmid DNA was purified using the Hispeed Plasmid Maxi Kit (QIAGEN, Toronto, ON). Cx47-GFP sequence was confirmed by sequencing and showed that Cx47 was fused with the amino terminus of GFP with a 19 amino acid linker (5'-GGRWLASWVPRARDPPVAT-3'). Six Cx47 mutants Cx47^{I46M}-GFP, Cx47^{G149S}-GFP, Cx47^{G236R}-GFP, Cx47^{G236S}-GFP, Cx47^{M286T}-GFP and Cx47^{T398I}-GFP cDNAs were generated using the site-directed mutagenesis approach with corresponding forward and reverse primers (see Table 2-1 for details). The cDNA was purified using the Hispeed Plasmid Maxi Kit (QIAGEN, Toronto, ON), and sequencing analysis confirmed the sequence of each fusion construct and the 19 amino acid linker.

Cx47 Mutants	Forward Primer (5'-3')	Reverse Primer (5'-3')
Cx47^{I46M}-GFP	CGGCGAGGCCATGT ACTCGGACGAG	CTCGTCCGAGTACAT GGCCTCGCCG
Cx47^{G149S}-GFP	GAGCCCATGCTGAG CCTGGGCGAGG	CCTCGCCCAGGCTC AGCATGGGCTC
Cx47^{G236R}-GFP	TACCTGCTGTACCGC TTCGAGGTGC	GCACCTCGAAGCGG TACAGCAGGTA
Cx47^{G236S}-GFP	TACCTGCTGTACAG CTTCGAGGTGC	GCACCTCGAAGCTG TACAGCAGGTA
Cx47^{M286T}-GFP	ACCTCTGTGAGACG GCCACCTGGG	CCCAGGTGGGCCGT CTCACAGAGGT
Cx47^{T398I}-GFP	CGGGCAGTGCTATC TCTGCGGGCAC	GTGCCC GCAGAGAT AGCACTGCCCG

Table 2-1. Primers used to generate Cx47 mutants. The forward and reverse primers for the generation of the Cx47 mutants, Cx47^{I46M}-GFP, Cx47^{G149S}-GFP, Cx47^{G236R}-GFP, Cx47^{G236S}-GFP, Cx47^{M286T}-GFP and Cx47^{T398I}-GFP, are listed.

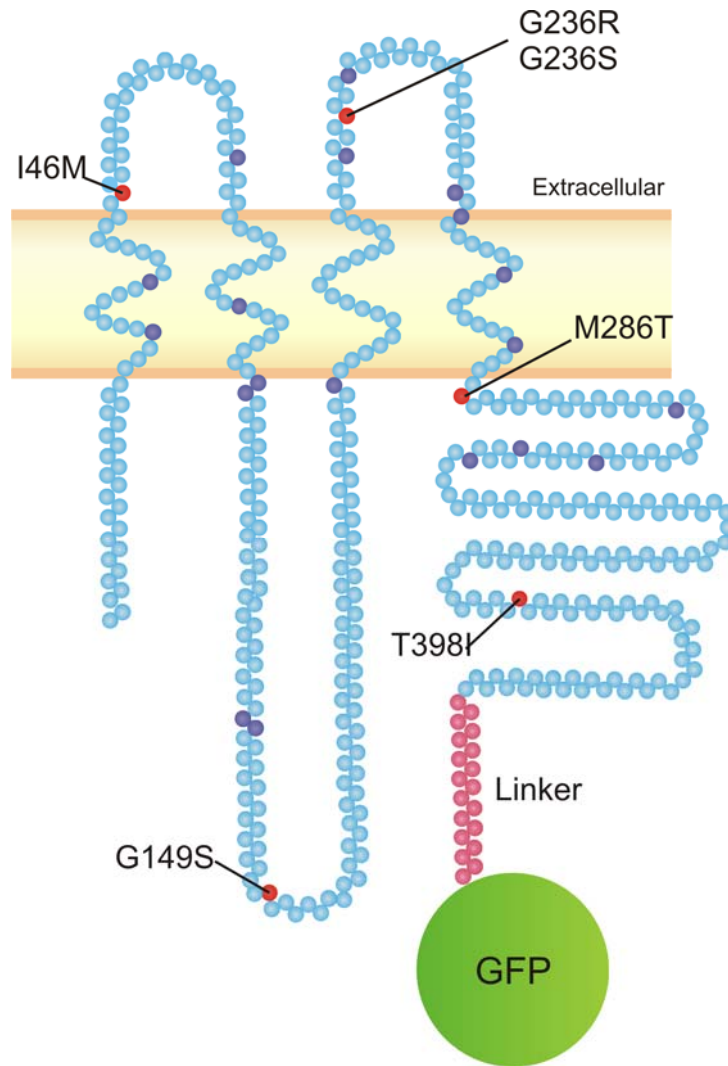


Figure 2-1. Human Cx47-GFP topology and mutant map. Twenty-four mutants have been identified from PMLD patients, and six mutations (red) were selected for the present study. These mutations are located in different domains of Cx47. Cx47 and the mutant constructs were tagged with GFP at the C-terminus via a 19 amino acid linker.

2.2. Connexin43 cDNA construct generation

The rat Cx43-monomeric red fluorescent protein (rCx43-mRFP) plasmid (Roger Tsien Lab, PNAS:99:7877-7882, 2002) was used for making the human Cx43-mRFP construct. The rCx43 gene was replaced by hCx43 at KpnI and BamHI sites of the rCx43-mRFP plasmid to generate the hCx43-mRFP construct. The WT hCx43 was isolated from the hCx43-GFP plasmid using KpnI and BamHI digestions (Norclone Biotech Labs, London, ON). Sequencing was used to confirm the fusion construct of hCx43-mRFP, which contains a 3 amino acid linker (5'-KDP-3') between hCx43 and mRFP.

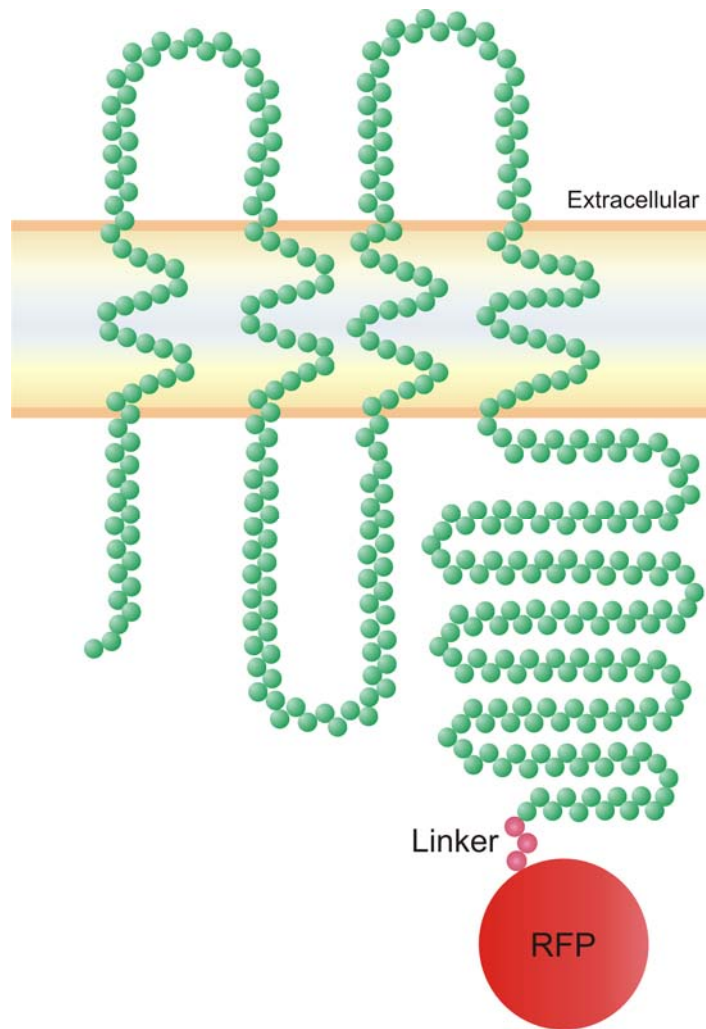


Figure 2-2. Human Cx43-mRFP topology. Human Cx43 construct was engineered to have a fluorescent protein tag, monomeric red fluorescent protein (mRFP), at the C-terminus via a 3 amino acid linker.

2.3. Cell culture and Transfection

N2A and HeLa cells were grown in Dulbecco's modified Eagle's medium (DMEM) containing high glucose, 2 mM L-glutamine but no sodium pyruvate supplemented with 10% fetal bovine serum and 1% penicillin and streptomycin sulphate, in a humidified atmosphere of 95% O₂ and 5% CO₂ at 37°C. N2A and HeLa cells were plated at 60-80% confluence on a 35 mm Petri dish 12-24 hours before transfection. For each transfection of Cx47 and mutants, cells were incubated with 1.25 µg of DNA and 2 µg of X-tremeGENE HP DNA transfection reagent (Roche, Mississauga, ON) in OPTIMEM I + GlutaMAX-I medium supplemented with HEPES and 2.4 g/L sodium bicarbonate (Invitrogen, Burlington, ON) for 4 hours, and the medium was then changed back to modified DMEM. For transfection of Cx43-mRFP, 2.5 µg of DNA and 3 µg of the transfection reagent were used due to lower mRFP expression efficiency. In each experiment, Cx47 and free GFP were transfected individually as positive and negative controls, respectively. For heterotypic studies, Cx43-mRFP and free red fluorescent protein (RFP) were also transfected individually to serve as positive and negative controls, respectively. Twenty-four hours after transfection, Cx47-GFP or mutant expressing cells were mixed with Cx43-RFP expressing cells for positive control and experimental groups, respectively. For the negative control, free GFP-expressing cells were mixed with free RFP-expressing cells. The cells were transferred onto coverslips 24 hours after transfection, and fixation for localization study or dual patch recordings was performed.

2.4. Fixation and Fluorescent Imaging

Cells transfected with Cxs were fixed with 80% methanol and 20% acetone solution for 10 minutes at -20°C. The coverslips were mounted on glass slides using Vectashield mounting medium with DAPI for nuclei staining (Vector, Burlington, ON). Cells were imaged on a Zeiss LSM 510-META confocal microscope (Thornwood, NY) mounted on an inverted Axiovert 200 motorized stage equipped with a 63x oil immersion objective (1.4 numerical apertures).

2.5. Electrophysiological recordings

24 hours after transfection, N2A cells were plated onto coverslips at 40-50% confluence. After 0.5-1 hour, coverslips were transferred to a recording chamber and bathed in an external solution (in mM: NaCl, 135; KCl, 5; HEPES, 10; MgCl₂, 1; CaCl₂, 2; BaCl₂, 1; CsCl, 2; Na pyruvate, 2; D-glucose, 5; pH 7.2). The cells were then visualized on a Leica DM IRB inverted microscope and green fluorescing cell pairs in close apposition were chosen for dual patch clamp recordings. For heterotypic pairs, cell pairs of red and green fluorescing cells in intimate contact were chosen. Glass pipettes were pulled into patch pipettes on a Narishige PC-10 pipette puller (Narishige, East Meadow, NY). Patch pipettes were filled with internal recording solution (mM: CsCl, 130; EGTA, 10; CaCl₂, 0.5; Mg-ATP, 5; HEPES, 10, pH 7.2) and the resistance was in the range of 2-5 MΩ. In order to measure channel conductance and V_j-gating, dual whole-cell voltage clamps were applied using two Axopatch 200B amplifiers and pClamp 9.0 software (Molecular Devices, Sunnyvale, California). Each cell of a pair was initially held at a common

holding potential of 0 mV. While one cell was held at 0 mV, the other cell of the pair was subjected to a series of positive and negative voltage steps from 0 mV to ± 100 mV with increments of 20 mV for 7 s to establish a transjunctional voltage (V_j) gradient at an interval of 8-23s between steps, and the junctional current (I_j) was measured in the other cell (Fig 2-3). Macroscopic transjunctional conductance (G_j) was calculated by dividing the measured junctional current by transjunctional voltage ($G_j = I_j / V_j$). The G_j for each cell pair at + or -20 mV was calculated and presented as mean \pm standard error of mean (SEM). For V_j -gating analysis, the peak and steady state at each voltage step were measured, and each steady-state was normalized to the corresponding peak to obtain the steady-state to peak ratio ($G_{j,ss}$). The $G_{j,ss}$ - V_j relationship for each polarity was then fitted individually by a two-state Boltzmann equation according to:

$$G_{j,ss} = \{(G_{\max} - G_{\min}) / (1 + \exp[A(V_j - V_o)])\} + G_{\min}$$

where V_o represents the voltage at which the conductance is half maximal, G_{\max} is the maximum normalized conductance, and G_{\min} is the normalized steady-state conductance. A defines the steepness of voltage sensitivity.

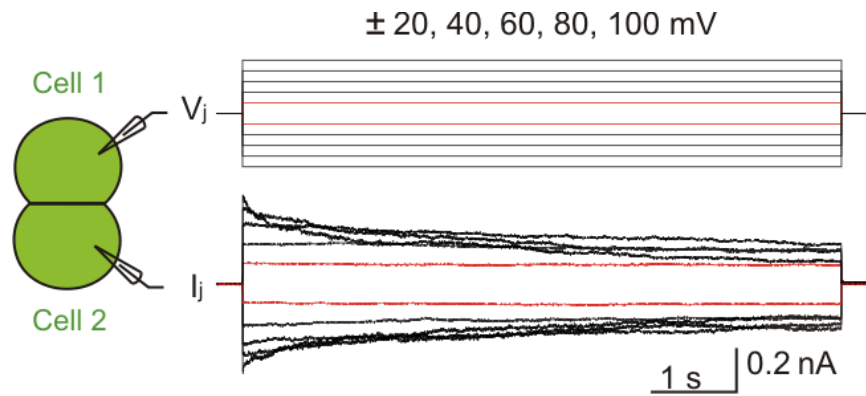


Fig 2-3. Dual whole-cell patch clamp. A pair of GFP-positive cells was selected and initially voltage-clamped at a common holding potential of 0 mV. A series of voltage steps ranging from ± 20 to ± 100 mV with 20 mV increment was generated in cell 1 to create transjunctional voltage gradient (V_j), and the junctional currents (I_j) recorded from cell 2 were analyzed and presented.

2.6. Statistical analysis

Group statistics were expressed as mean \pm standard error of mean (SEM). The Kruskal-Wallis test followed by Dunn's multiple comparison test was performed to compare multiple groups of data for statistical difference. The differences were considered significant at $P < 0.05$. All statistical data were obtained from GraphPad Prism 4.0 (San Diego, CA, USA). Significant differences were denoted as *, ** or *** for $P < 0.05$, $P < 0.01$ or $P < 0.001$, respectively, when compared to the wildtypes.

3. Results

3.1. Cx47 formed homotypic GJ plaque-like structures in HeLa cells, and showed transjunctional voltage-dependent gating (V_j -gating) in N2A cells.

To facilitate the study of localization and functional characterization of Cx47, green fluorescent protein (GFP) was fused at the carboxyl terminus of Cx47, forming Cx47-GFP. Gap junction-deficient HeLa cells were transiently transfected with the Cx47-GFP construct, and the green fluorescent signals were detected in the intracellular compartments as well as at the cell-cell junction to form GJ plaque-like structures (Fig 3-1A). This observation indicated that GFP-tagging was not altering the ability of Cx47 to localize to cell-cell interface.

The transjunctional voltage-dependent gating (V_j -gating) properties of homotypic Cx47 channels were studied by dual whole-cell patch clamp technique in N2A cells transiently transfected with Cx47-GFP. A pair of GFP-positive cells was selected and initially held at a common holding potential of 0 mV. One cell of the pair was stepped to a series of positive and negative voltage steps from 0 mV to ± 20 -100 mV with increments of 20 mV to establish the transjunctional voltage gradient (V_j), and the junctional currents (I_j) were measured in the other cell (Fig 3-1B). At the V_j of ± 20 and ± 40 mV, the amplitude of I_j was relatively constant. At the voltage steps of ± 60 mV, the I_j amplitude started to decline with time symmetrically with respect to positive and negative V_j -polarities to steady-state levels. As the V_j was increased to ± 80 and ± 100 mV, the junctional current showed more prominent inactivation and faster gating.

For each voltage step, the steady-state junctional conductance (G_j) was normalized to its corresponding peak G_j to obtain $G_{j,ss}$, and plotted against V_j ($n = 5$,

Fig 3-1C). Cx47-GFP channels showed increasing sensitivity to V_j and faster V_j -gating as the absolute V_j gradient was increased. For the negative polarity, the $G_{j,ss}$ - V_j relationship of Cx47-GFP homotypic channels was characterized by producing Boltzmann parameters, G_{\max} of 1.01 ± 0.03 , G_{\min} of 0.18 ± 0.11 , V_o of 70.98 ± 5.151 mV and A of 0.066 (Table 3-1). For the positive polarity, the Boltzmann parameters were as follows: $G_{\max} = 1.02 \pm 0.06$, $G_{\min} = 0.26 \pm 0.12$, $V_o = -62.41 \pm 6.6$ mV, and $A = 0.065$.

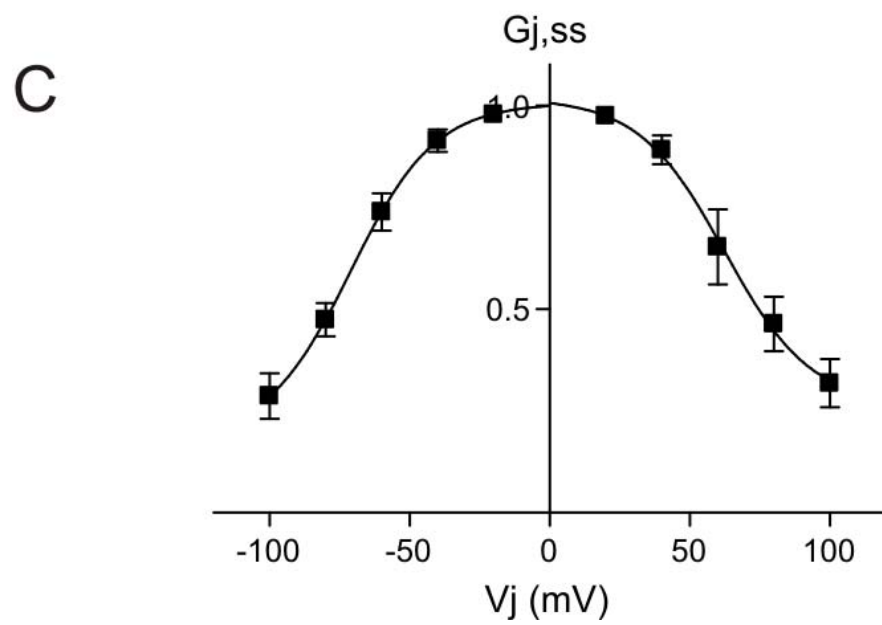
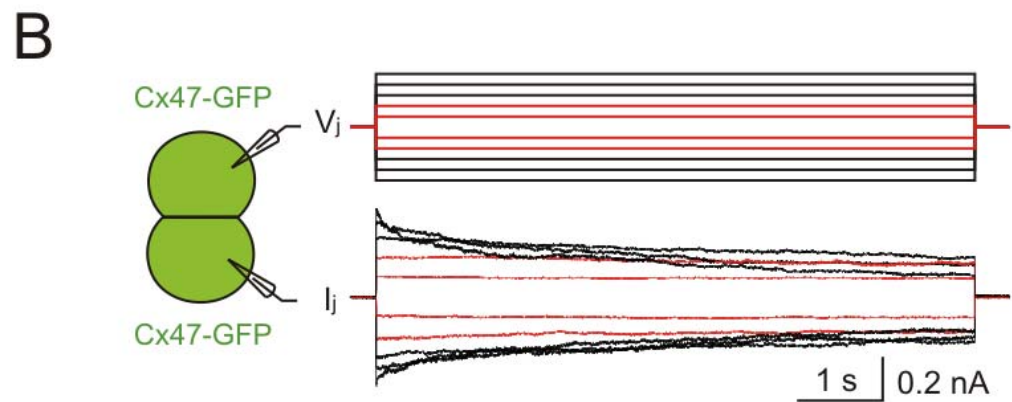
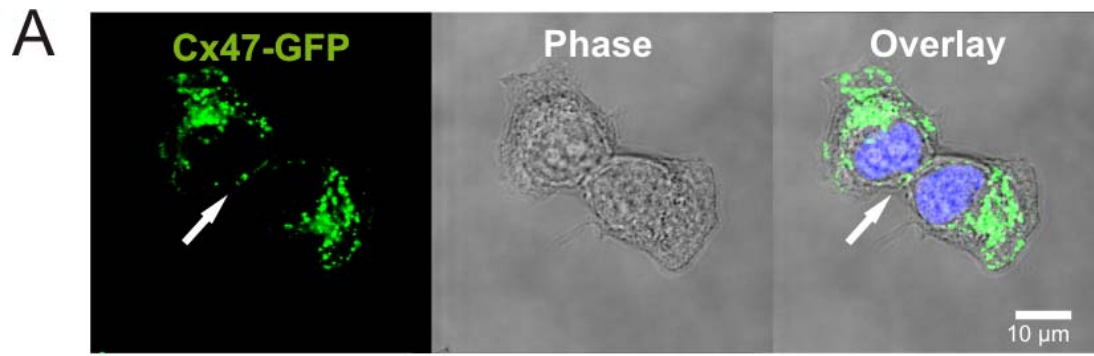


Figure 3-1. The localization and macroscopic V_j -gating properties of Cx47-GFP homotypic gap junctions. (A) A representative confocal image of Cx47-GFP is shown (left panel). A phase contrast image (middle panel) and an overlaid image (right panel) are also shown. GFP was observed in the intracellular regions and at the cell-cell interface (white arrow). (B) A voltage step protocol (from 0 mV to \pm 20-100 mV with 20 mV increments) was applied to characterize V_j -gating properties in N2A cells. One cell of a pair underwent the protocol, while the other cell was held at 0 mV to establish V_j . In the cell held at 0 mV, the junctional current (I_j) was recorded, and the representative junctional current traces of Cx47-GFP gap junctions in response to the protocol are shown. V_j at \pm 20 to \pm 40 mV voltage steps and the corresponding I_j s are shown in red traces with little V_j -gating. (C) Normalized junctional conductance ($G_{j,ss}$, steady-state relative to maximal) was plotted as a function of V_j and fit with Boltzmann equation. The mean $G_{j,ss}$ at each V_j was calculated and represented as mean \pm SEM ($n = 5$), and the Boltzmann fitted curves (smooth lines) are shown in solid lines.

Construct	G_{max}	G_{min}	V_o (mV)	A	V_j
Cx47-GFP/	1.0 ± 0.06	0.3 ± 0.1	62.4 ± 6.6	0.065	+
Cx47-GFP	1.0 ± 0.03	0.2 ± 0.1	71.0 ± 5.2	0.066	-
Cx47-GFP/	1.0 ± 0.02	0.1 ± 0.02	55.84 ± 1.3	0.12	+
Cx43-mRFP	n/a	n/a	n/a	n/a	-

Values for V_o and A are absolute values. n/a; not applicable

Table 3-1. Boltzmann parameters of Cx47/Cx47 and Cx47/Cx43 channels. The Boltzmann parameters of homotypic Cx47/Cx47 and heterotypic Cx47/Cx43 channels at positive and negative polarities are shown. When Cx43 expressing cells of heterotypic cell pairs underwent the voltage-step protocol, the data could not be fitted with Boltzmann equation at negative V_j polarities.

3.2. All Cx47 mutants tested were able to form homotypic GJ plaque-like structures in HeLa cells.

The cellular localization of the GFP-tagged Cx47 mutants, I46M, G149S, G236R, G236S, M286T and T398I was comparable to WT Cx47, such that the fluorescent signals were detected mostly in the cytoplasm. The localization at the cell-to-cell interface was also detected in HeLa cells (Fig 3-2). The dominance of intracellular distribution could be due to either GFP tagging and/or overexpression. The ability of these mutants to reach the cell-cell interface provided further directions for functional characterizations through dual patch clamp recordings.

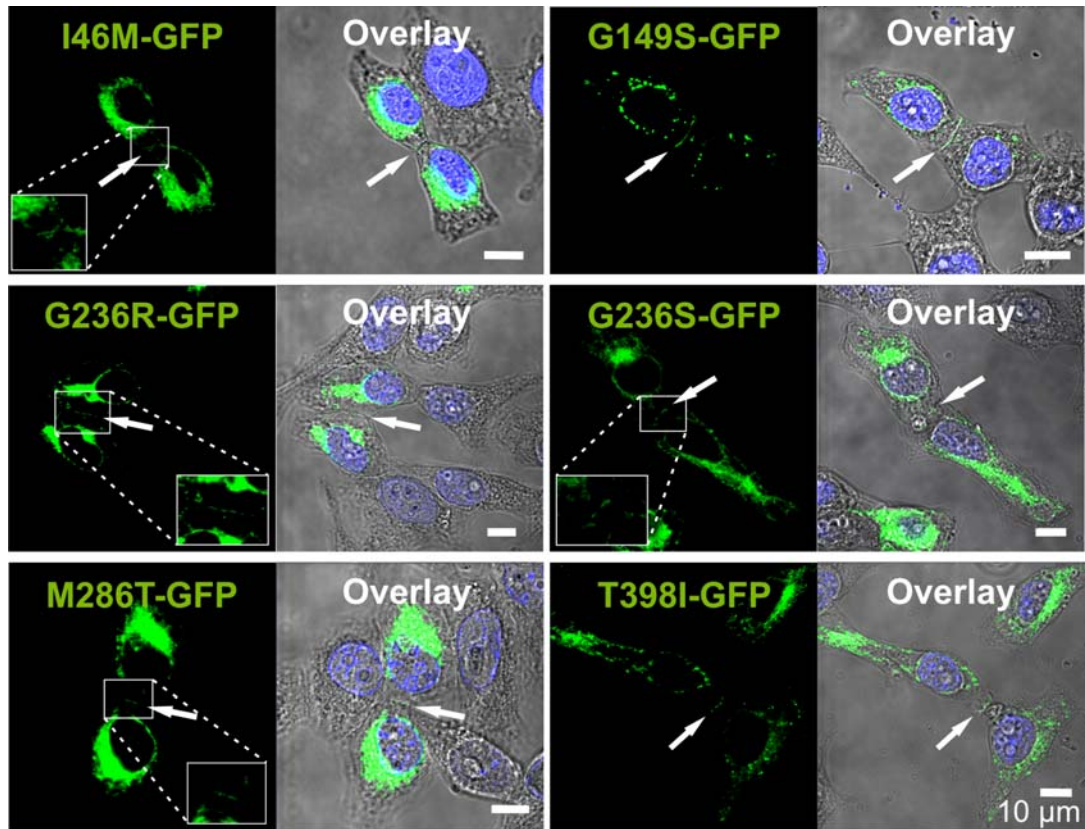


Figure 3-2. Localization of Cx47 mutants in HeLa cells. The cellular localization of Cx47 mutants indicated by GFP signals was detected under a confocal microscope. All six mutants (I46M, G149S, G236R, G236S, M286 and T398I) appeared to localize at the cell-cell interface, albeit with abundant intracellular localization. Fluorescent image (1st panel); overlay of fluorescent image with DAPI staining (blue) and phase image to show cell morphology (2nd panel).

3.3. Four out of six PMLD-linked Cx47 mutants tested failed to form functional homotypic GJ channels.

Dual whole-cell patch clamp recordings were applied to N2A cells expressing Cx47 mutants - I46M, G149S, G236R, G236S, M286T or T398I - to analyze the functional status of Cx47 mutant homotypic GJs. The representative junctional current traces of the six mutant homotypic channels at -20 mV are illustrated in Figure 3-3A. Unlike the cells expressing WT Cx47, the I_j s were not detected in N2A cell pairs expressing the mutants I46M, G236R, G236S or M286T. In contrast, I_j s were recorded in N2A cell pairs expressing G149S or T398I demonstrating that these two mutants were able to form functional homotypic GJ channels. The G_j of G149S (3.8 ± 0.8 nS) was similar to that of wild-type Cx47 (6.4 ± 1.1 nS; $P > 0.05$). The mean G_j of T398I-expressing cell pairs (1.9 ± 0.8 nS) was lower than but not significantly different from that of the WT ($P > 0.05$).

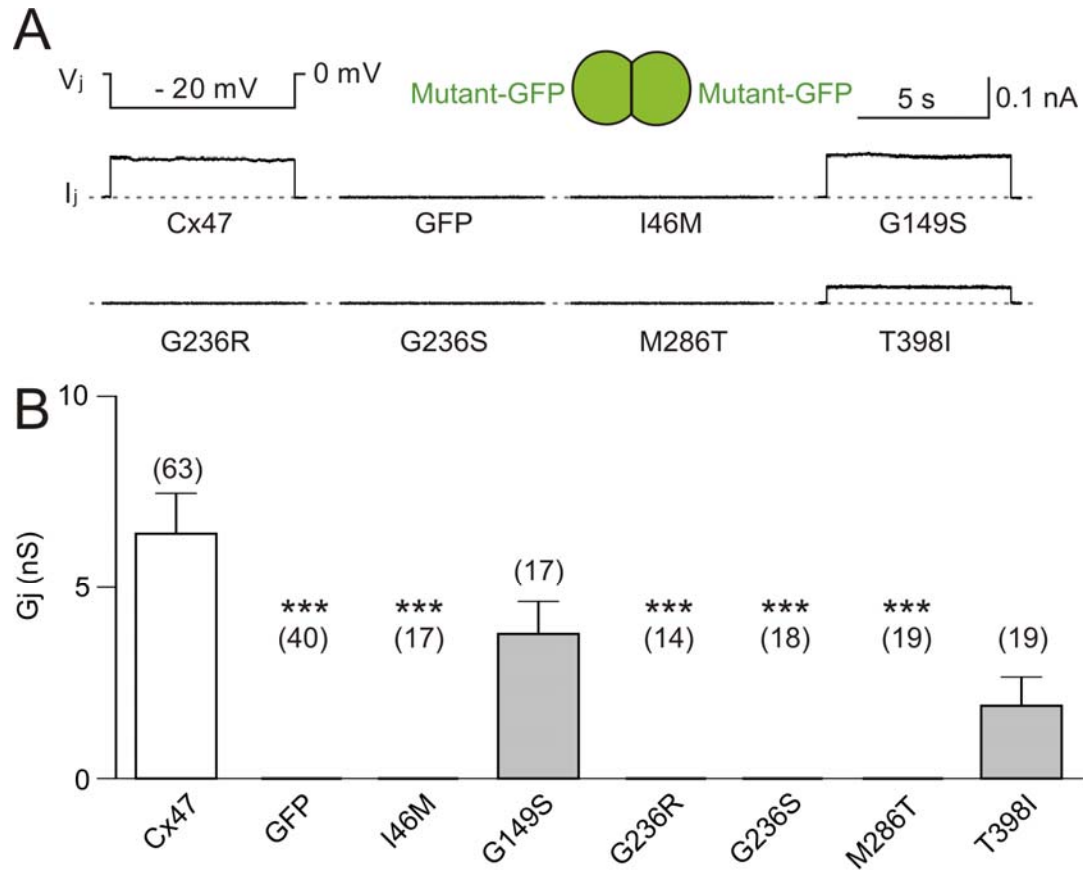


Figure 3-3. Junctional conductance (G_j) measurements of Cx47 mutant homotypic channels. (A) Representative macroscopic junctional current traces elicited from N2A cell pairs expressing one of the six Cx47 mutants (I46M, G149S, G236R, G236S, M286T and T398I) in response to $V_j = -20$ mV. Similar to WT Cx47, I_j s were detected only in G149S and T398I. Like GFP, the negative control, no apparent I_j was detected for the other four mutants. (B) The mean G_j of homotypic channels of Cx47 mutants. The mean G_j s of G149S and T398I homotypic channel were not significantly different from that of WT Cx47. The number above each bar indicates the total number of cell pairs recorded. These recordings were obtained from 3 to 10 batches of transfections.

3.4. Both Cx47^{G149S} and Cx47^{T398I} GJ channels showed V_j-gating properties similar to those of Cx47.

To identify if the functional GJ channels formed by G149S or T398I possess any channel property changes in V_j-gating, I measured G_j responses to V_js from ± 20 to ± 100 mV for each of these two homotypic mutant GJ channels. As shown in Fig. 3-4, both G149S and T398I showed relatively constant junctional current at ± 20 and ± 40 mV. As the absolute values of V_j were increased, the G_j showed symmetrical decay to steady-state levels at both polarities, and greater V_j-dependent inactivation with increasing absolute V_j values. These V_j-dependent inactivations were similar to that of WT Cx47 homotypic channels (Fig 3-1B).

In order to quantify the sensitivity of G149S and T398I homotypic channels to V_j, the steady-state G_j was normalized to their corresponding peak G_j to obtain G_{j,ss}, and plotted against V_js. The G_{j,ss}-V_j plot for G149S (Fig. 3-4C, n = 3) and T398I (Fig. 3-4D, n = 3) did not show obvious differences in V_j-sensitivity from that of wild-type Cx47 GJ channels (smooth lines in Fig. 3-4C, D), indicating that the GJ V_j-gating properties were not altered by these two mutations.

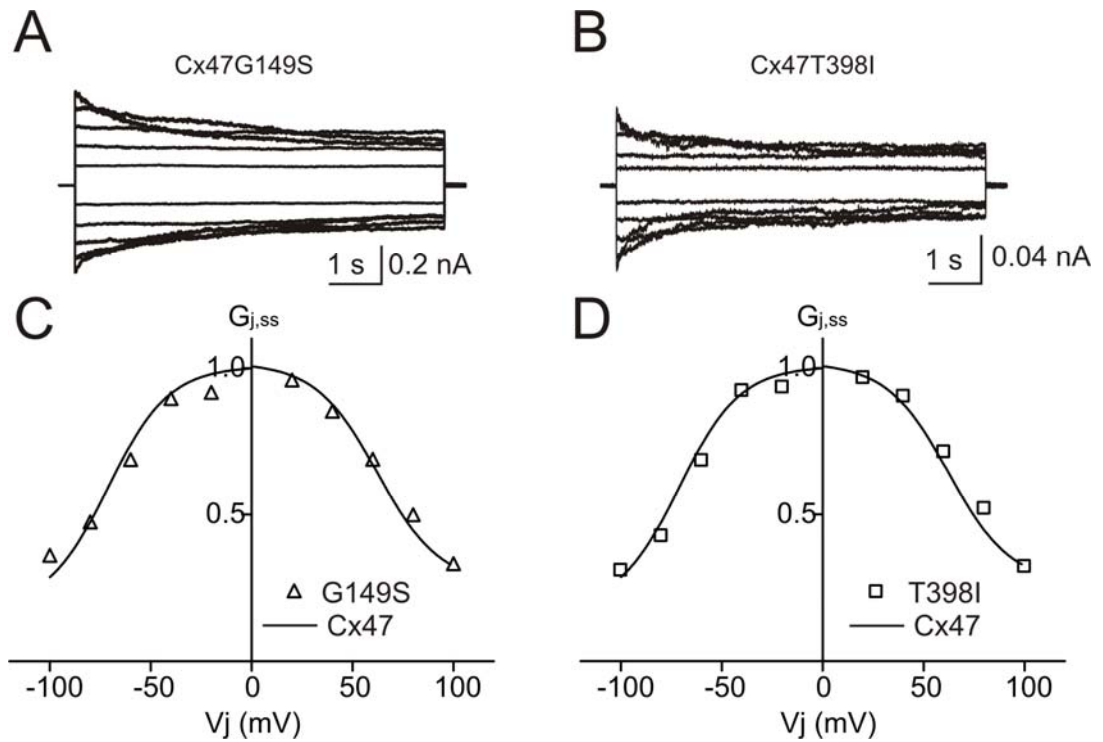


Figure 3-4. V_j -gating properties of G149S and T398I homotypic gap junctions.

(A) Representative and superimposed junctional currents in a N2A cell pair expressing G149S are shown in response to the same voltage protocols as shown in Fig. 3-1B. (B) Representative and superimposed junctional currents of T398I homotypic channels in N2A cells are shown. (C) Normalized junctional conductance ($G_{j,ss}$) of G149S channels (open triangle) was plotted against V_j , and superimposed onto wild-type Cx47 homotypic channel Boltzmann fitting curves (smooth lines). (D) Normalized junctional conductance ($G_{j,ss}$) of T398I channels (open squares) was plotted against V_j , and superimposed onto wild-type Cx47 channel Boltzmann fitting curves (smooth lines). Both G149S and T398I channels failed to show any major differences in V_j -sensitivity and V_j -gating trends as compared with WT Cx47 channels.

3.5. Cx47 and Cx47^{G149S} formed heterotypic gap junction plaque-like structures with Cx43 in HeLa cells.

The localization of Cx47 and Cx47^{G149S} in heterotypic cell pairs with Cx43 was examined in HeLa cells to determine whether they can co-localize at the cell-cell junction. Cx47-GFP (or Cx47^{G149S}-GFP) and Cx43-mRFP were localized in intracellular regions and partially co-localized at the cell-cell interfaces in both Cx47/Cx43 and Cx47^{G149S}/Cx43 heterotypic pairs. The overlap of GFP and RFP at the cell-to-cell interfaces produced yellow colour (arrows and boxes in Fig. 3-5), indicating both WT Cx47 and the G149S mutant were able to co-localize with Cx43 at cell-cell junctions.

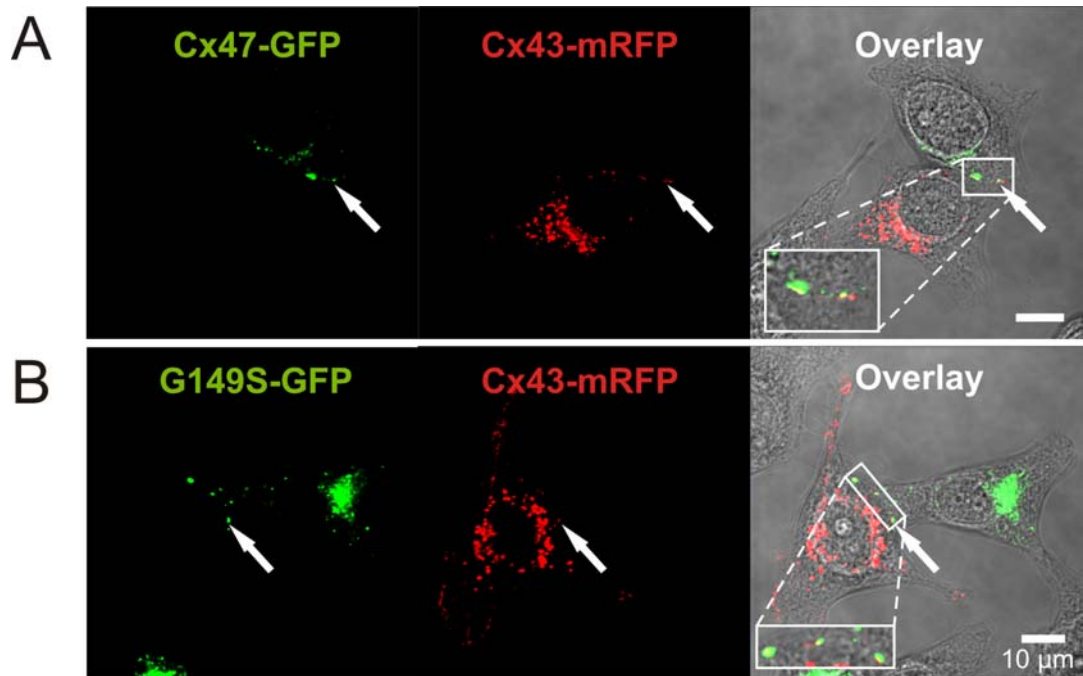


Figure 3-5. Co-localization of Cx47 (or Cx47^{G149S}) and Cx43-mRFP at cell-cell interfaces in HeLa cell pairs. Cx47-GFP (or Cx47^{G149S}-GFP) and Cx43-mRFP were expressed separately and then plated together to allow them to pair up. Co-localization of Cx47-GFP (A) [or Cx47^{G149S}-GFP (B)] and Cx43-mRFP was observed at the cell-cell junction in Cx47-GFP [or Cx47^{G149S}-GFP] and Cx43-mRFP expressing HeLa cells. White arrows and enlarged box areas were used to highlight the partial co-localization at the cell-cell interface.

3.6. V_j -gating of Cx47/Cx43 heterotypic channels.

The V_j -gating properties of Cx47-GFP/Cx43-mRFP heterotypic channels were studied in N2A cell pairs where a GFP-positive cell was paired with an RFP-positive cell. The same V_j -step protocols were used to study Cx47/Cx43 heterotypic channels (Fig 3-6A). When the cell expressing Cx43 was pulsed to increasingly positive V_j , the G_j of Cx47/Cx43 channels showed rapid and large inactivation to steady states (Fig. 3-6A). However, when the cell expressing Cx43 was pulsed to negative V_j , the G_j showed either no or very minimal inactivation and the gatings were very slow in the tested V_j s (Fig. 3-6A top traces). When the V_j -step protocols were applied to Cx47-expressing cells, the Cx47/Cx43 channels showed similar gating trends but at the opposite V_j polarities (Fig. 3-6A bottom traces), compared to when V_j -step protocols were applied to cells expressing Cx43.

I constructed a $G_{j,ss}$ - V_j plot ($n = 5$, Fig 3-6B) and the $G_{j,ss}$ - V_j relationship showed a strong difference in the sensitivity to V_j depending on the polarity of the V_j in Cx47/Cx43 channels. When a Cx43 expressing cell was stepped to positive V_j s, the junctional current inactivated substantially to a low residual conductance. At this V_j polarity, we could fit the data with the Boltzmann equation with G_{max} of 0.98 ± 0.02 , G_{min} of 0.10 ± 0.02 , V_o of 55.84 ± 1.3 mV and A of 0.12. Cx47/Cx43 channels showed lower residual conductances and V_o and greater V_j -sensitivity, when compared to Cx47/Cx47 homotypic channels. On the contrary, when Cx43 expressing cells were stepped to negative voltages, little inactivation was observed and the data could not be described by Boltzmann distribution.

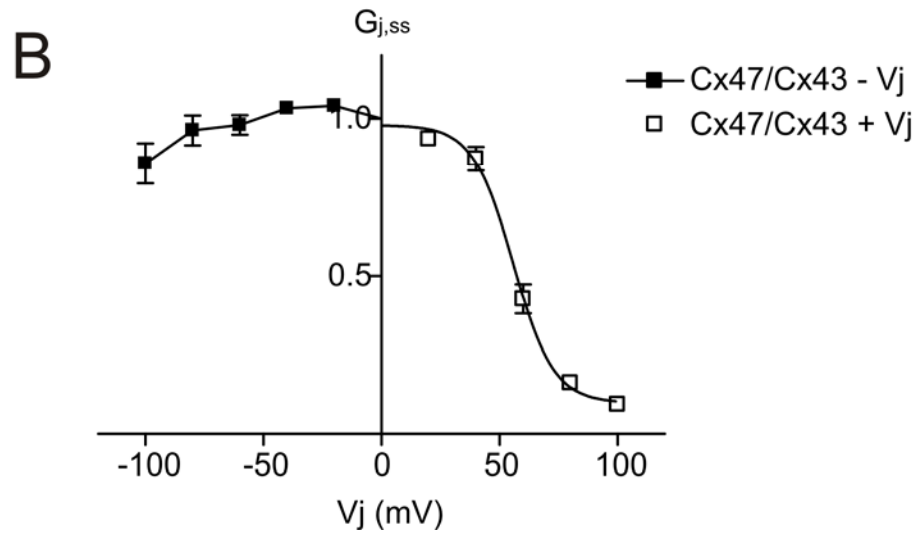
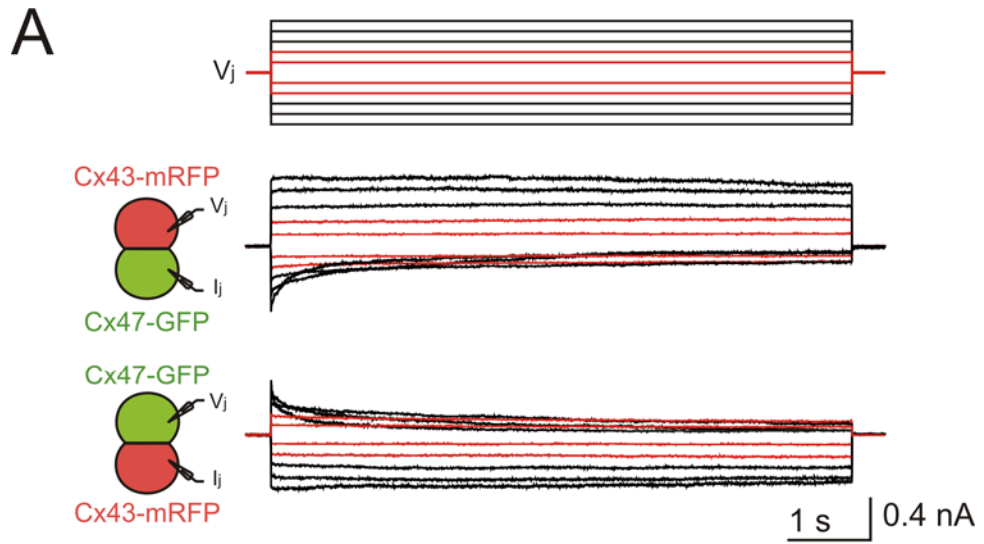


Figure 3-6. V_j -gating properties of Cx47/Cx43 heterotypic gap junctions. (A) A Cx47-GFP-expressing cell (green) and Cx43-mRFP expressing cell (red) pair was selected for patch clamp recording. A voltage step protocol (from 0 mV to ± 20 to ± 100 mV) was applied to the cell expressing Cx43-mRFP, and the I_j s from the cell expressing Cx47-GFP are presented (top traces). When the same voltage step protocol was applied to a Cx47-GFP-expressing cell, the junctional current traces showed similar gating kinetics but at the opposite V_j polarities (bottom traces), compared to when the protocol was applied to the cell expressing Cx43-mRFP. (B) Normalized junctional conductance ($G_{j,ss}$, steady-state relative to maximal) was plotted as a function of V_j . The $G_{j,ss}$ - V_j relationship at positive polarity on the Cx43 side was well-fitted with the Boltzmann equation ($n = 5$). The mean $G_{j,ss}$ at each V_j was calculated and represented as mean \pm SEM.

3.7. The majority of the selected Cx47 mutants failed to form functional heterotypic channels with Cx43 in N2A cells

The major gap junction type between oligodendrocytes and astrocytes is Cx47/Cx43 heterotypic channels. To study if the mutations in Cx47 (I46M, G149S, G236R, G236S, M286T and T398I) have any functional impact on Cx47/Cx43 GJ channels, I measured G_j in Cx47/Cx43 heterotypic GJ channels in N2A cell pairs expressing a Cx47 mutant in one and Cx43 in the other (Fig. 3-7). The representative I_j traces of the six mutant heterotypic channels at 20 mV are illustrated in Figure 3-7A. Similar to that observed for Cx47 mutant homotypic GJ channels, the majority of the Cx47 mutant/Cx43 heterotypic cell pairs were either completely uncoupled ($P < 0.001$; $G_j = 0$ nS for Cx47^{G236R}/Cx43 and $G_j = 0.01 \pm 0.01$ nS for Cx47^{M286T}/Cx43) or showed substantially reduced G_j s ($G_j = 0.06 \pm 0.03$ nS for Cx47^{G236S}/Cx43 ($P < 0.001$) and $G_j = 0.51 \pm 0.28$ nS for Cx47^{I46M}/Cx43, $P < 0.01$). Two of the mutants, G149S and T398I, were able to form functional heterotypic GJs ($G_j = 9.36 \pm 2.54$ nS and 7.05 ± 2.79 nS respectively) with comparable G_j s to those of WT Cx47/Cx43 channels ($G_j = 6.24 \pm 1.13$) in N2A cells ($P > 0.05$).

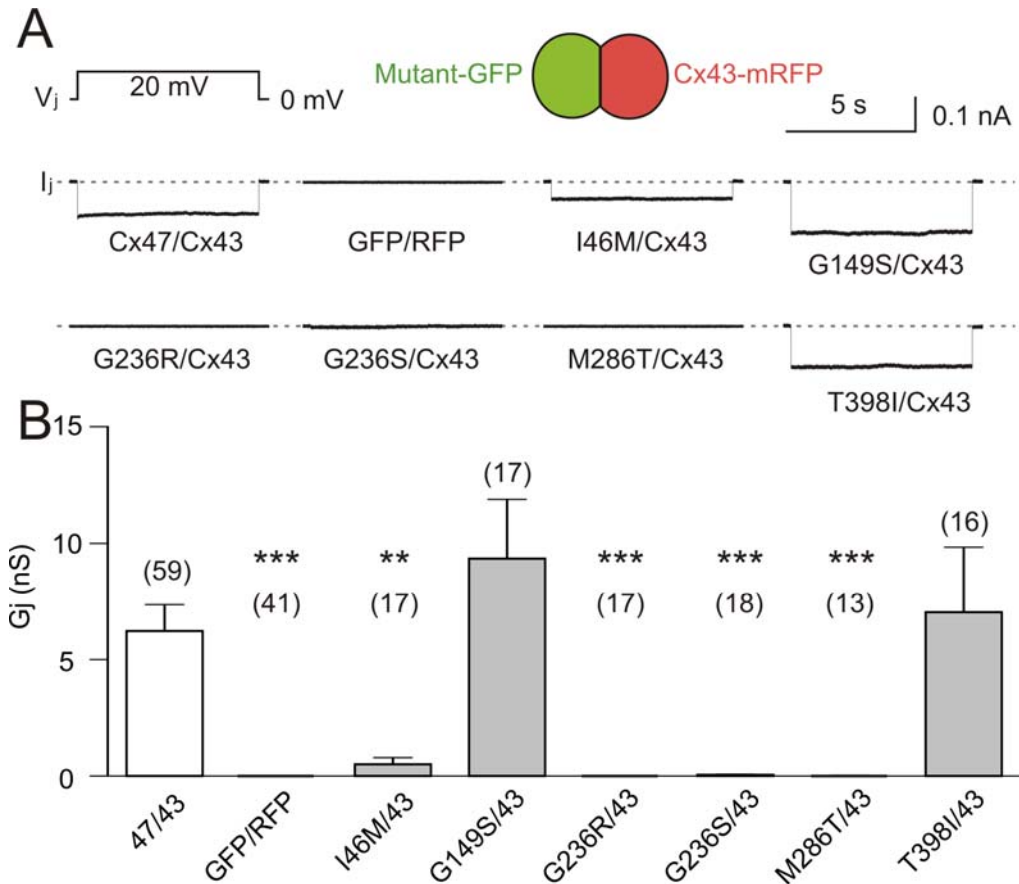


Figure 3-7. Junctional conductance (G_j) measurements of Cx47 mutant heterotypic channels with Cx43. (A) Representative macroscopic junctional current traces of Cx47 mutant (I46M, G149S, G236R, G236S, M286T and T398I) heterotypic channels with Cx43 in response to a 20 mV voltage step. (B) The mean G_j s of Cx47 mutant/Cx43 heterotypic channels are shown as a bar graph. I46M, G236R, G236S and M286T heterotypic channels showed significantly reduced junctional conductance from Cx47/Cx43 channels in N2A cells. G149S and T398I heterotypic channel G_j s were not significantly different from that of WT Cx47/Cx43. The number of cell pairs analyzed is shown above each bar. Data in each bar were obtained from 3-10 independent transfections. GFP expressing cell and RFP expressing cell pairs (GFP/RFP) were used as negative control.

3.8. V_j -gating properties of functional Cx47 mutant/Cx43 heterotypic channels.

To further study if there is any obvious defect in V_j -gating properties in those functional (G149S and T398I) or occasionally functional (I46M) Cx47 mutant/Cx43 heterotypic GJ channels, the V_j -gating properties were studied in cell pairs expressing the Cx47 mutant-GFP in one and Cx43-mRFP in the other.

When the cell expressing Cx43 was pulsed to increasingly positive V_j , the junctional currents of I46M/Cx43, G149S/Cx43 and T398I/Cx43 heterotypic channels showed rapid and large inactivation to steady states (Fig. 3-8A-C). However, when the cell expressing Cx43 was pulsed to negative V_j , the junctional current showed little or no inactivation and the kinetics were very slow in the tested V_j s (Fig. 3-8A-C). These V_j -dependent inactivations were similar to that of WT Cx47/Cx43 heterotypic channels (Fig 3-8A). The steady-state junctional conductances were normalized to their corresponding peak junctional conductances to obtain $G_{j,ss}$ and plotted against V_j (Fig 3-8 D-F). Preliminary data obtained from Cx47^{I46M}/Cx43 (n = 2), Cx47^{G149S}/Cx43 (n = 1) and Cx47^{T398I}/Cx43 (n = 1) did not show any major difference in the V_j -gating sensitivity from that of Cx47/Cx43 channels (Fig. 3-8 D-F).

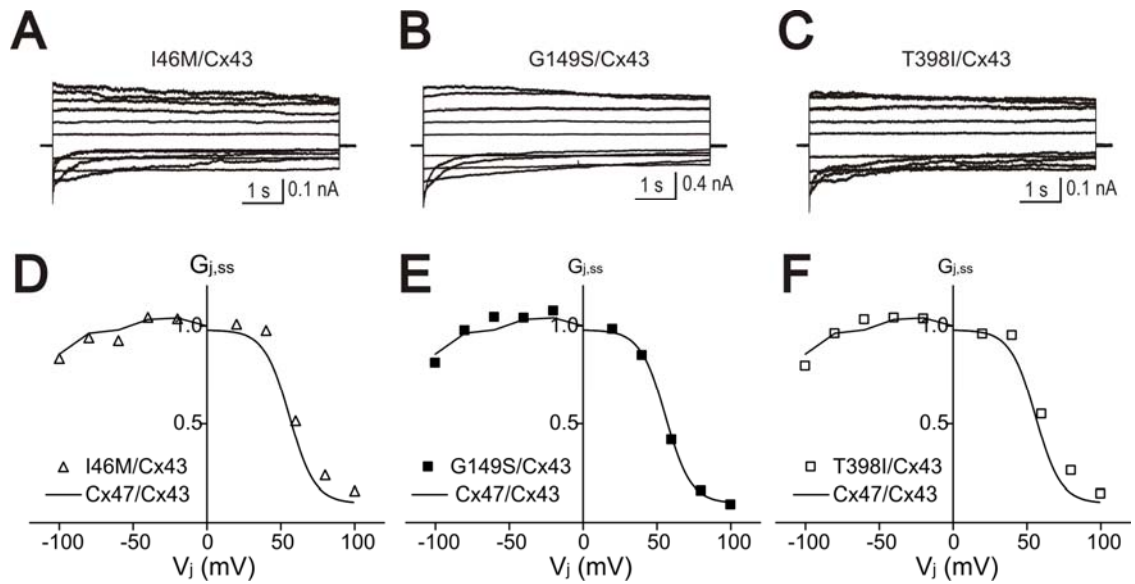


Figure 3-8. V_j -gating properties of Cx47 mutant/Cx43 heterotypic gap junctions.

(A-C) Representative junctional currents recorded in N2A cell pairs expressing Cx47^{I46M} (A), Cx47^{G149S} (B) or Cx47^{T398I} (C) in one and Cx43-mRFP in the other in response to a voltage step protocol applied to cells expressing Cx43 (identical to that described in Fig. 3-6A). (D-F) Normalized junctional conductance ($G_{j,ss}$) of Cx47^{I46M} (open triangle), Cx47^{G149S} (filled square) and Cx47^{T398I} (open square) heterotypic channels with Cx43 are plotted against V_j , and superimposed on the WT Cx47/Cx43 channel Boltzmann fitting curves (smooth lines). None of I46M, G149S and T398I heterotypic channels showed drastic differences in V_j -gating sensitivity and inactivation kinetics compared with WT Cx47/Cx43 heterotypic channels (shown as smooth lines in panel D, E and F).

4. Discussion

4.1. Overall study

In this study, the localization and functional status of Cx47 mutants that are associated with the central hypomyelinating disease PMLD were studied using a confocal microscopy and dual whole-cell patch clamp. These two approaches were highly effective in studying the localization of Cxs by observing the cellular distribution of GFP or mRFP tags at the C-termini and the GJ channel function by measuring the coupling conductance and probing V_j -gating properties. Based on previous studies, I proposed that PMLD-linked Cx47 mutations (I46M, G149S, G236R, G236S, M286T and T398I) would interrupt GJIC via homotypic Cx47/Cx47 and/or heterotypic Cx47/Cx43 gap junction channels.

Heterologous expression in gap junction-deficient HeLa and N2A cells showed that all the tested Cx47 mutants appeared to be localized intracellularly with a small portion at the cell-cell junctions (Table 4-1). Mutants I46M, G236R, G236S and M286T did not form functional homotypic channels. Although few heterotypic pairs expressing the I46M, G236S or M86T Cx47 mutants with WT Cx43 showed low levels of coupling, the overall mean G_j s were not significantly different from the negative control. In contrast, mutants G149S and T398I formed both functional homotypic and heterotypic channels whose G_j s were similar to those observed in WT Cx47/Cx47 and Cx47/Cx43 channels. Although no apparent defects of the two mutants were observed in their homotypic channels and heterotypic GJs with Cx43, it was previously shown that the two mutants may have defects in their hemichannel functions (Diekmann et al., 2010).

These experimental data showed that the majority of the selected Cx47 mutations

cause disruption in GJIC via Cx47/Cx47 and/or Cx47/Cx43 channels. The results in the model system suggest that the mutations may interrupt oligodendrocyte coupling to each other and with astrocytes, and affect the maintenance of normal CNS myelination by oligodendrocytes.

Mutants	Localization at apposing membranes	Formation of Homotypic GJs	Homotypic GJ V_j-gating	Heterotypic GJs	Heterotypic GJ V_j-gating
I46M	+	-	n/a	-	no change*
G149S	+	+	no change	+	no change
G236R	+	-	n/a	-	n/a
G236S	+	-	n/a	-	n/a
M286T	+	-	n/a	-	n/a
T398I	+	+	no change	+	no change

+ = yes, - = no, n/a = not applicable, *no apparent changes were observed.

Table 4-1. Summary of localization and functional status of Cx47 mutants. All mutants were observed at cell-cell interfaces. However, the selected Cx47 mutants, except G149S and T398I, failed to form functional Cx47/Cx47 homotypic and Cx47/Cx43 heterotypic channels. In contrast, G149S and T398I successfully formed functional homotypic and heterotypic channels whose macroscopic G_js and V_j-gating were similar to WT Cx47/Cx47 and Cx47/Cx43 channels.

4.2. Localization of Cx47-GFP at the cell-cell interface

In order to visualize the localization of Cxs, GFP was tagged at the C-terminus of Cx47 and its mutants. In HeLa cells, Cx47-GFP was observed in the intracellular regions and at the cell-cell junctions. The observation of Cx47-GFP at the cell-cell interface suggests that tagged Cx47 is able to traffic to the cell membrane and form gap junction plaque-like structures, similar to that of untagged Cx47 detected using Cx47 antibody (Diekmann et al., 2010; Orthmann-Murphy et al., 2007a). The heavy localization of GFP within the cell is likely due to overexpression of GFP-fused Cx47. However, this heavy intracellular distribution raises possibility that GFP tagging may affect the trafficking of Cx47 to the membrane.

Similar to WT Cx47, the selected GFP-tagged PMLD-linked Cx47 mutants were observed to localize in intracellular regions as well as at the cell-cell interface, suggesting possible formation of GJ plaques. Previous study of untagged G149S, M286T and T398I also showed that all three mutants readily traffic to the cell surface and form GJ plaque-like structures in HeLa cells. Furthermore, the three mutants were co-localized with an endoplasmic reticulum (ER) marker against ER protein disulfide isomerase (Diekmann et al., 2010) or an ER chaperone GRP94 (Orthmann-Murphy et al., 2007a). The localization pattern of these previous studies is consistent with the present study, and gives a possible explanation for the heavy intracellular localization of Cx47 and its mutants. However, although all mutants were observed at the cell-cell junctions at the light microscopy level, it cannot be concluded that they all form GJ plaques and functional channels. Therefore, a functional approach using dual whole-cell patch clamp recording was applied.

4.3. Homotypic Cx47-GFP gap junction channels and PMLD mutants

Dual whole-cell patch clamp recordings indicated that Cx47-GFP is able to form functional homotypic GJ channels in N2A cells. It was previously reported that GFP tagging at the C-terminus of mouse Cx47 does not affect functional properties of untagged mCx47 homotypic GJ channels in terms of single channel conductance, V_j -gating and dye permeability (Teubner et al., 2001). Human Cx47-GFP channels in our model system showed similar V_j -gating trends but less sensitivity to V_j , compared to previously studied untagged hCx47 channels (Orthmann-Murphy et al., 2007a). These differences are likely due to the differences at the NT of cDNA constructs used. Our Cx47 construct starts from the first AUG codon, which encodes the full length of human Cx47, while the construct used by Orthmann-Murphy and colleagues started from the second AUG codon, which is short of 9 nucleotides encoding the first 3 amino acid residues (Orthmann-Murphy et al., 2007a). It was noted that expression of full length Cx47 or the construct without the first 3 amino acid residues, can form functional channels, but they possess distinct V_j -gating and pH-gating properties (Fasciani et al., 2011). It is also possible that hCx47 that we used is different from mCx47. Although the effect of GFP tagging has not been directly studied, our observations indicate that Cx47-GFP is able to form functional homotypic channels in N2A cells without drastic changes in the macroscopic conductance and V_j -gating properties.

Most PMLD-linked Cx47 mutants (I46M, G236R, G236S and M286T) studied in our model system resulted in loss-of-function in coupling likely due to impairment of homotypic channels. Structural homology modeling of Cx47 based on Cx26

crystal structure showed that the I46M mutation, located in the M1/E1 boundary, may affect the salt bridge formation between E1 and E2 critical for maintaining the correct orientation of E2 in the formation of a connexon (Biancheri et al., 2012). Furthermore, the structural modelling of hCx26 and the mutations at the M1/E1 border residues indicated that the residues at the M1/E1 boundary are involved in size restriction and voltage sensing (Maeda et al., 2009; Verselis et al., 1994). Thus, it is possible that the I46M mutation interrupted the pore formation and, ultimately, impaired homotypic channel function. Similarly, less flexible residues were introduced by mutations G236R and G236S in E2. Both E1 and E2 are known to be involved in the docking of two connexons to form a gap junction channel (Biancheri et al., 2012; Maeda et al., 2009). Similar to I46M, the two E2 mutations, G236R and G236S, may interfere with the normal pore formation and/or docking, impairing the formation of functional channels (Biancheri et al., 2012). The failure of the M286T mutant to form functional homotypic channels was consistent with a previous study using the same mutant without a fluorescent protein tag (Orthmann-Murphy et al., 2007a). The homology structural modeling indicates that the introduction of a polar residue in the mutant M286T may change the local hydrophobic properties of TM4 and interrupt the channel function (Biancheri et al., 2012). Although the four non-functional Cx47 mutants appeared to be able to localize at the cell-cell junction, they failed to form functional channels. This suggests that the mutations may inhibit channel function by changing the docking of their hemichannels or the structure components critical for the function of GJ channels.

The previous study also showed that PMLD linked mutants P90S, Y272D and M286T failed to form functional homotypic GJs, possibly due to partial accumulation of the mutants in the ER (Orthmann-Murphy et al., 2007a). The partial accumulation of the mutants in the ER may be one possible mechanism that prevents the formation of functional channels for the four mutants I46M, G236R, G236S and M286T in N2A cells. Also, the GFP tagging at the C-termini may affect the trafficking of Cx47 and the mutants, leading to the high intracellular localization. Due to the spatial resolution limitation of our confocal microscopy, we cannot fully rule out the possibility that some of the observed putative gap junction plaques may not be localized at the apposing membranes, but in intracellular regions near the cell-cell junction.

In contrast to the other Cx47 mutants, G149S and T398I formed functional homotypic channels in N2A cells. Both G149S and T398I homotypic channels showed no difference from the WT channels in terms of macroscopic conductance and V_j -gating sensitivity. G149S is located in the intracellular loop domain and may not directly affect the pore formation, which may explain the ability of G149S to form functional channels as opposed to the mutants found in the extracellular loops (I46M, G236R and G236S) (Biancheri et al., 2012). It has previously been addressed that GJs in oligodendrocytes and astrocytes participate in buffering of K^+ released during neuronal activities, which may create V_j between cells (Menichella et al., 2006). Although I could not obtain sufficient amount of V_j -gating data to perform a proper Boltzmann fit, no clear difference was shown in V_j -gating properties obtained from two pairs of cells of the two mutants, G149S and T398I,

when compared to that of the WT. This preliminary test suggests that the two mutants may respond to V_j similar to that of the WT channels. However, it is still possible that the two mutants have a minor effect that could not be detected by our system. Also, they may interrupt other properties such as pH-sensitivity, hemichannel activities, or their interaction with regulatory proteins such as zonula occludens-1 (ZO-1), ZO-1-associated nucleic acid-binding protein and multi-PDZ domain protein 1, and regulate gene expression, oligodendrocyte differentiation and survival (Li et al., 2004; Li et al., 2008; Penes et al., 2005). Furthermore, oligodendrocytes *in vivo* may behave differently from N2A and HeLa cells. Although T398I homotypic channels did not show statistically significant difference from the WT, a reduction in the macroscopic junctional conductance was observed. This could be explained by a reduced number of channels being formed at the cell-cell junctions, reduced single channel conductance, or both. Based on macroscopic conductance, all mutants except G149S caused complete or partial defect in their homotypic channel functions, which may play a role leading PMLD.

4.4. Co-localization of Cx47-GFP and Cx43-mRFP at the cell-cell interface

In order to be able to select heterotypic cell pairs, Cx43 was tagged with mRFP at the C-terminus. Cx43-mRFP fusion protein has been used for localization studies and is able to assemble into functional GJ channels (Campbell et al., 2002; Gong et al., 2007). In my study, localization observations demonstrated that Cx47-GFP and Cx43-mRFP can form heterotypic GJ plaque-like structures between adjoining HeLa cells. The yellow colour indicated that the green and red fluorescent signals

co-localized at the apposing membranes. A similar observation was reported in a previous study where immunostaining was used to determine untagged Cx47 and Cx43 localization (Orthmann-Murphy et al., 2007b). The immunolabeling study illustrated co-localization of the two Cx antibodies using different fluorescent colours, suggesting that these Cxs may have a chance to form heterotypic GJ channels (Orthmann-Murphy et al., 2007b). These observations of similar localization patterns reflect that the fluorescent protein tagging at both Cx47 and Cx43 had no major effect on their localization to the cell-cell interfaces.

Due to the low probability of observing co-localization of both Cx47 and Cx43, I did not study all Cx47 mutants. However, with the mutant tested (Cx47^{G149S}-GFP), it clearly showed co-localization with Cx43-mRFP at the cell-cell junction, forming small clusters of GJ plaque-like structures, similar to its WT counterpart. However, due to spatial resolution limitations, the co-localization of the two Cxs does not demonstrate the formation of real heterotypic GJ channels.

4.5. Heterotypic Cx47-GFP/Cx43-mRFP gap junction channels and PMLD mutants

Dual patch clamp recordings revealed that Cx47-GFP and Cx43-mRFP can form functional heterotypic GJ channels. Cx47/Cx43 heterotypic GJs showed asymmetric V_j -gating properties, where Cx47 hemichannels were conspicuously more sensitive to V_j . In a previous study where the fluorescent proteins were not fusion-linked to 3 amino acid-short Cx47 and Cx43, the clear V_j -gating at both polarities was observed with little asymmetry in the gating kinetics as the absolute

value of V_j was increased (Orthmann-Murphy et al., 2007b). I, however, observed clear rectification. This difference in V_j -gating could be attributed to different Cx47 translation initiation codons and/or the fluorescent tags at the C-termini of Cxs.

When the first three residues of Cx47 were eliminated, the asymmetric rectification with the V_j -polarity in full-length Cx47/Cx43 heterotypic channels was reported to no longer exist (Fasciani et al., 2011). This may explain the less asymmetric V_j -gating in the previous study, compared to the present study.

In homotypic channels, Cx43-mRFP induces similar macroscopic junctional conductance to Cx43-GFP. This Cx43-GFP, in turn, exhibits similar macroscopic and single channel conductance as untagged Cx43, but less sensitivity to V_j compared to untagged Cx43, due to lack of fast V_j -gating (Bukauskas et al., 2001). Cx43-mRFP has not been directly compared to untagged Cx43; it is possible that mRFP tagging at the C-terminus of Cx43 has little effect on trafficking to the cell surface and formation of functional GJs, but significantly affects V_j -sensitivity, similar to GFP tagging. This may contribute to the rectification of Cx47-GFP/Cx43-mRFP channels, as opposed to Cx47/Cx43 channels where the fluorescent proteins were linked via internal ribosome entry site (IRES).

Two of the PMLD-linked Cx47 mutants analyzed (G149S and T398I) showed no obvious difference in macroscopic conductance and V_j -gating properties in their heterotypic channels. Like in homotypic channels, G149S and T398I did not disturb the normal Cx47/Cx43 heterotypic GJ functions. Thus, both G149S and T398I may contribute to PMLD through other mechanisms such as hemichannels, rather than interrupting Cx47/Cx47 and Cx47/Cx43 GJIC by oligodendrocytes and astrocytes

in the CNS.

The four mutant (I46M, G236R, G236S and M286T) heterotypic channels with Cx43-mRFP displayed no coupling conductance, which is the same as the negative controls where only GFP and RFP were expressed. I46M located at the M1/E1 border showed coupling in 1/4 of the recorded cell pairs. In heterotypic GJs, the use of the chimera approach demonstrated that E1 of Cx46 faces the lumen and determines the channel conductance (Trexler et al., 2000). This further suggests that I46M may affect the structure of the pore, and consequently impairs GJ coupling in homotypic channels. It seems possible however, to rarely stabilize the interaction of Cx47^{I46M} and Cx43 hemichannels, and cause partial rescue in heterotypic GJ functions, whose V_j-gating kinetics are not different from the WT. Also, the G236S mutation in E2 domain reduced coupling level and caused asymmetry in V_j-gating in some pairs. E2 is the primary domain that determines heterotypic compatibility (Nakagawa et al., 2011; White et al., 1994; White et al., 1995). Likewise, it is possible that G236S may cause spatial changes at the docking interface and affect E2-E2 interactions in the formation of a complete channel. Consequently, it may interrupt the channel function completely in homotypic channels, but partially in heterotypic channels with Cx43. Interestingly, G236R showed no coupling in all heterotypic pairs tested as opposed to G236S. This can be explained by the difference in charge and size between the two amino acids, arginine and serine. However, despite the formation of functional channels, the majority of the pairs tested were not coupled. It is not clear why some pairs are functional, while others are not. It is unlikely due to that unidentified endogenous Cxs contributed to the GJ

channel formation with Cx43, as we routinely use free GFP/RFP pairs as negative controls for our functional tests. Whenever, we saw coupling in negative controls, we trashed all data from that batch of transfections. Also, if these mutant Cxs have the ability to reach cell-cell junctions and form heterotypic GJs with Cx43, it is possible that the mutants may occasionally stabilize the coupling between the two cells. Overall, the reduction in the macroscopic conductance and the possibility of forming functional heterotypic channels may account for interruption in GJIC between oligodendrocytes and astrocytes, causing PMLD.

4.6. PMLD-linked Cx47 mutants and hemichannel functions

A connexon (hemichannel) may behave on its own as an aqueous pore at the unopposed cell surface. Hemichannels mediate the exchange of ions and small molecules with the extracellular environment and may play a role in Ca^{2+} wave propagation (Goodenough and Paul, 2003; Saez et al., 2010). Although the exact role of hemichannels in oligodendrocytes has not been addressed, PMLD-linked mutants have been reported to affect hemichannel functions due to loss-of-function and change in membrane potential in a model system. In such a study, G149S resulted in loss of hemichannel function in *Xenopus laevis* oocytes (Diekmann et al., 2010). This suggests that G149S may not affect gap junction functions, but does affect hemichannel activities, which may consequently interrupt initiation of Ca^{2+} waves to adjacent oligodendrocytes and astrocytes and affect other cellular processes. In the same study, T398I displayed hemichannel currents comparable to Cx47, but the cells expressing T398I had depolarized membrane potential

(Diekmann et al., 2010). Hemichannels can be opened at positive membrane potentials. Also, the correlation of increased hemichannel open probability with cell death was shown in Cx26 and Cx32 mutant expressing cells (Liang et al., 2005; Stong et al., 2006). Furthermore, Cx43 hemichannel opening causes ATP release, which ultimately increases susceptibility of the cells to injury and death (Saez et al., 2010; Tong et al., 2007). Accordingly, T398I likely affects oligodendrocytes by increasing the hemichannel activities.

Based on my data, G149S and T398I did not show obvious defect in their homotypic and heterotypic GJs. The increased or loss of hemichannel activity may provide another possible cause for the disease, leading to impairment of GJIC among oligodendrocytes as well as between oligodendrocytes and astrocytes.

4.7. Clinical phenotypes of Cx47 mutants

Patients with the selected Cx47 mutations showed clinical phenotypes of nystagmus, progressive spasticity, ataxia, developmental delay and white matter changes in the CNS, irrespective of the age of onset (Bugiani et al., 2006; Henneke et al., 2008; Uhlenberg et al., 2004; Wang et al., 2010). Cx47 is highly expressed in oligodendrocytes and mediates O/O and O/A coupling in the CNS. Thus, it was postulated that mutations in Cx47 affect Cx47/Cx47 and/or Cx47/Cx43 GJIC. Interestingly, all of the selected mutants that resulted in loss-of-function in their homotypic and heterotypic GJs caused the disease only when recessively inherited (Henneke et al., 2008; Uhlenberg et al., 2004; Wang et al., 2010). In contrast, both G149S and T398I that formed functional homotypic and heterotypic channels with

Cx43 were able to cause the disease in the heterozygous state, i.e. autosomal dominant (Henneke et al., 2008). Furthermore, the patient with G149S and one of the two patients carrying T398I achieved a lower score in their best motor function compared to patients carrying the non-functional mutants I46M or M286T (Biancheri et al., 2012). These genotypes and their associated clinical phenotypes indicate that G149S and T398I have dominant and more detrimental effects on oligodendrocyte function than others.

Based on my observations, the two mutants are likely to have no conspicuous defects in GJ functions in terms of macroscopic conductance and V_j -gating in N2A cells. Likewise, G149S and T398I may affect different mechanisms such as hemichannel activities rather than GJs in oligodendrocytes *in vivo*, and consequently, cause PMLD through their dominant effects.

4.8. Cx47 is the critical Cx that constitutes oligodendrocyte-to-oligodendrocyte GJs.

Previous studies using a dye coupling approach in Cx knock-out and mutant mice models have illustrated that oligodendrocytes are coupled to each other. When the Cx47 gene was knocked out in mice, a pronounced reduction in O/O coupling was observed in the corpus callosum (Maglione et al., 2010; Tress et al., 2011). In homozygous Cx47^{M286T/M286T} mice, the number of cells coupled to the dye-injected oligodendrocyte was significantly reduced (Tress et al., 2011). This loss-of-function of M286T *in vivo* might have interrupted GJs between oligodendrocytes, and is in parallel with our observation that homotypic M286T GJ coupling was completely abolished in the model system. Furthermore, these mice models demonstrate the

functional importance of Cx47 in O/O coupling *in vivo*.

In humans, mutations in Cx47 alone were enough to cause neurological and behavioural symptoms (Uhlenberg et al., 2004; Wang et al., 2010). Conversely, in mice models, the ablation of Cx47 alone or Cx32 alone did not manifest obvious phenotypic abnormalities (Menichella et al., 2003; Nelles et al., 1996; Odermatt et al., 2003). The conspicuous behavioural abnormalities with severe demyelination in the CNS were observed only in mice lacking both Cx47 and Cx32 (Menichella et al., 2003; Odermatt et al., 2003). Also, the dye coupling studies showed that O/O coupling was completely abolished in mouse corpus callosum in Cx47 and Cx32 double-knock out mice (Maglione et al., 2010). In the neocortex, O/O coupling in Cx32-deficient mice was more affected than in Cx47-deficient mice (Wasseff and Scherer, 2011). These differences among individual Cx knock-out and the double knock-out mouse models demonstrate the functional redundancy of both Cxs in oligodendrocyte coupling in mice. Likewise, a similar phenomenon was observed in Cx47^{M286T/M286T} and Cx47^{M286T/M286T}/Cx32^{-/-} mice (Tress et al., 2011). The different phenotypes between humans and mouse models can be explained by different physiological mechanisms. In humans, mutations in Cx32 lead to X-linked demyelinating peripheral neuropathy (Charcot-Marie-Tooth disease type 1). Accordingly, Cx47 likely has a more significant contribution to the oligodendrocyte functions than Cx32 in humans. Therefore, the PMLD-linked mutants alone may interrupt O/O coupling and ultimately, oligodendrocyte function in maintaining central myelin.

4.9. Cx47 is critical for O/A coupling.

As oligodendrocytes and astrocytes express different Cx sets, O/A coupling is mediated by heterotypic gap junctions. In Cx47-deficient mice, O/A coupling was significantly compromised in the corpus callosum and neocortex, whereas it remained relatively unaffected in Cx32-deficient mice (Maglione et al., 2010; Wasseff and Scherer, 2011). Similar to O/O coupling, O/A coupling was completely abolished in Cx32 and Cx47 double-deficient mice (Maglione et al., 2010). In astrocyte Cx knock-out mice, O/A coupling was not affected by the deletion of astrocyte-specific Cx43 but when both Cx43 and Cx30 were deleted (Maglione et al., 2010). Thus, it can be concluded that functional redundancy of glial Cx also exists in O/A coupling, possibly by Cx47/Cx43, Cx47/Cx30, Cx32/Cx30 and Cx32/Cx26 GJs (Altevogt and Paul, 2004; Magnotti et al., 2011; Orthmann-Murphy et al., 2007b).

It is widely known that O/A coupling is mediated by Cx47/Cx43 and Cx32/Cx30 heterotypic GJs, the former being dominant (Orthmann-Murphy et al., 2007b). In the knock-out mouse models described above, O/A coupling was affected more in Cx47-null mice compared to Cx32-null or Cx43-null mice (Maglione et al., 2010; Wasseff and Scherer, 2011). This suggests the functional importance of Cx47 in O/A coupling, and further, of Cx47/Cx43 heterotypic GJs at the O/A junctions. The homozygous M286T mice showed pronounced reduction in the number of cells coupled to dye-injected oligodendrocytes (Tress et al., 2011). This may include not only neighbouring oligodendrocytes, but also astrocytes, suggesting the impairment of GJs both at O/O and O/A junctions. Therefore, Cx47 is the most critical Cx that

enables O/O and O/A GJIC. Consequently, PMLD-associated mutations in Cx47 may significantly affect the O/A coupling *in vivo* and interrupt the oligodendrocyte functions in maintaining normal myelin, as shown in our model system.

4.10. Conclusion

Our dual whole-cell patch clamp analysis revealed that the selected PMLD-linked Cx47 mutants have complete or partial defects in Cx47/Cx47 and/or Cx47/Cx43 GJ coupling functions. Although all the selected mutants were able to localize to the cell-cell interface, the majority of them resulted in loss of function. Both G149S and T398I formed functional homotypic and heterotypic GJs with Cx43. In humans, Cx47 linked to central myelination is likely to have dominant action over Cx32 in oligodendrocyte function, as most Cx32 mutations are linked to peripheral neuropathy only. My work demonstrated that Cx47 mutants impaired Cx47/Cx47 and/or Cx47/Cx43 gap junctions in the model system. Further studies are necessary to understand glial Cx interactions and the exact molecular pathology of Cx mutations in CNS hypomyelination.

References

- Al-Achkar, W., F. Moassass, B. Al-Halabi, and A. Al-Ablog. 2011. Mutations of the Connexin 26 gene in families with non-syndromic hearing loss. *Mol Med Report*. 4:331-335.
- Altevogt, B.M., K.A. Kleopa, F.R. Postma, S.S. Scherer, and D.L. Paul. 2002. Connexin29 is uniquely distributed within myelinating glial cells of the central and peripheral nervous systems. *J Neurosci*. 22:6458-6470.
- Altevogt, B.M., and D.L. Paul. 2004. Four classes of intercellular channels between glial cells in the CNS. *J Neurosci*. 24:4313-4323.
- Arora, A., P.J. Minogue, X. Liu, P.K. Addison, I. Russel-Eggitt, A.R. Webster, D.M. Hunt, L. Ebihara, E.C. Beyer, V.M. Berthoud, and A.T. Moore. 2008. A novel connexin50 mutation associated with congenital nuclear pulverulent cataracts. *J Med Genet*. 45:155-160.
- Biancheri, R., C. Rosano, L. Denegri, E. Lamantea, F. Pinto, F. Lanza, M. Severino, and M. Filocamo. 2012. Expanded spectrum of Pelizaeus-Merzbacher-like disease: literature revision and description of a novel GJC2 mutation in an unusually severe form. *Eur J Hum Genet*.
- Bugiani, M., S. Al Shahwan, E. Lamantea, A. Bizzi, E. Bakhsh, I. Moroni, M.R. Balestrini, G. Uziel, and M. Zeviani. 2006. GJA12 mutations in children with recessive hypomyelinating leukoencephalopathy. *Neurology*. 67:273-279.
- Bukauskas, F.F., A. Bukauskiene, M.V. Bennett, and V.K. Verselis. 2001. Gating properties of gap junction channels assembled from connexin43 and connexin43 fused with green fluorescent protein. *Biophys J*. 81:137-152.
- Bukauskas, F.F., and V.K. Verselis. 2004. Gap junction channel gating. *Biochimica et biophysica acta*. 1662:42-60.
- Campbell, R.E., O. Tour, A.E. Palmer, P.A. Steinbach, G.S. Baird, D.A. Zacharias, and R.Y. Tsien. 2002. A monomeric red fluorescent protein. *Proc Natl Acad Sci U S A*. 99:7877-7882.
- Cao, F., R. Eckert, C. Elfgang, J.M. Nitsche, S.A. Snyder, H.u. DF, K. Willecke, and B.J. Nicholson. 1998. A quantitative analysis of connexin-specific permeability differences of gap junctions expressed in HeLa transfectants and *Xenopus* oocytes. *J Cell Sci*. 111 (Pt 1):31-43.
- Das Sarma, J., F. Wang, and M. Koval. 2002. Targeted gap junction protein constructs reveal connexin-specific differences in oligomerization. *J Biol Chem*. 277:20911-20918.
- Diekmann, S., M. Henneke, B.C. Burckhardt, and J. Gartner. 2010. Pelizaeus-Merzbacher-like disease is caused not only by a loss of connexin47 function but also by a hemichannel dysfunction. *Eur J Hum Genet*. 18:985-992.
- Fasciani, I., D. Gonzalez-Nieto, and L.C. Barrio. 2011. Molecular bases for the rectifying properties of heterotypic oligodendrocyte connexin47 and astrocyte connexin43 junctions. *In International Gap Junction Conference, Ghent, Belgium*. 150.
- Gemel, J., V. Valiunas, P.R. Brink, and E.C. Beyer. 2004. Connexin43 and connexin26 form gap junctions, but not heteromeric channels in co-expressing cells. *J Cell Sci*. 117:2469-2480.
- Gong, X.Q., Q. Shao, S. Langlois, D. Bai, and D.W. Laird. 2007. Differential potency of

- dominant negative connexin43 mutants in oculodentodigital dysplasia. *J Biol Chem.* 282:19190-19202.
- Goodenough, D.A., and D.L. Paul. 2003. Beyond the gap: functions of unpaired connexon channels. *Nat Rev Mol Cell Biol.* 4:285-294.
- Goodenough, D.A., and D.L. Paul. 2009. Gap junctions. *Cold Spring Harb Perspect Biol.* 1:a002576.
- Hanemann, C.O., C. Bergmann, J. Senderek, K. Zerres, and A.D. Sperfeld. 2003. Transient, recurrent, white matter lesions in X-linked Charcot-Marie-Tooth disease with novel connexin 32 mutation. *Arch Neurol.* 60:605-609.
- Henneke, M., P. Combes, S. Diekmann, E. Bertini, K. Brockmann, A.P. Burlina, J. Kaiser, A. Ohlenbusch, B. Plecko, D. Rodriguez, O. Boespflug-Tanguy, and J. Gartner. 2008. GJA12 mutations are a rare cause of Pelizaeus-Merzbacher-like disease. *Neurology.* 70:748-754.
- Kamasawa, N., A. Sik, M. Morita, T. Yasumura, K.G. Davidson, J.I. Nagy, and J.E. Rash. 2005. Connexin-47 and connexin-32 in gap junctions of oligodendrocyte somata, myelin sheaths, paranodal loops and Schmidt-Lanterman incisures: implications for ionic homeostasis and potassium siphoning. *Neuroscience.* 136:65-86.
- Kleopa, K.A., J.L. Orthmann, A. Enriquez, D.L. Paul, and S.S. Scherer. 2004. Unique distributions of the gap junction proteins connexin29, connexin32, and connexin47 in oligodendrocytes. *Glia.* 47:346-357.
- Kovacs, J.A., K.A. Baker, G.A. Altenberg, R. Abagyan, and M. Yeager. 2007. Molecular modeling and mutagenesis of gap junction channels. *Prog Biophys Mol Biol.* 94:15-28.
- Kunzelmann, P., W. Schroder, O. Traub, C. Steinhauser, R. Dermietzel, and K. Willecke. 1999. Late onset and increasing expression of the gap junction protein connexin30 in adult murine brain and long-term cultured astrocytes. *Glia.* 25:111-119.
- Li, X., A.V. Ionescu, B.D. Lynn, S. Lu, N. Kamasawa, M. Morita, K.G. Davidson, T. Yasumura, J.E. Rash, and J.I. Nagy. 2004. Connexin47, connexin29 and connexin32 co-expression in oligodendrocytes and Cx47 association with zonula occludens-1 (ZO-1) in mouse brain. *Neuroscience.* 126:611-630.
- Li, X., M. Penes, B. Odermatt, K. Willecke, and J.I. Nagy. 2008. Ablation of Cx47 in transgenic mice leads to the loss of MUPP1, ZONAB and multiple connexins at oligodendrocyte-astrocyte gap junctions. *The European journal of neuroscience.* 28:1503-1517.
- Liang, G.S., M. de Miguel, J.M. Gomez-Hernandez, J.D. Glass, S.S. Scherer, M. Mintz, L.C. Barrio, and K.H. Fischbeck. 2005. Severe neuropathy with leaky connexin32 hemichannels. *Ann Neurol.* 57:749-754.
- Loddenkemper, T., K. Grote, S. Evers, M. Oelerich, and F. Stogbauer. 2002. Neurological manifestations of the oculodentodigital dysplasia syndrome. *J Neurol.* 249:584-595.
- Maeda, S., S. Nakagawa, M. Suga, E. Yamashita, A. Oshima, Y. Fujiyoshi, and T. Tsukihara. 2009. Structure of the connexin 26 gap junction channel at 3.5 Å resolution. *Nature.* 458:597-602.
- Maglione, M., O. Tress, B. Haas, K. Karam, J. Trotter, K. Willecke, and H. Kettenmann. 2010. Oligodendrocytes in mouse corpus callosum are coupled via gap junction channels formed by connexin47 and connexin32. *Glia.* 58:1104-1117.

- Magnotti, L.M., D.A. Goodenough, and D.L. Paul. 2011. Functional heterotypic interactions between astrocyte and oligodendrocyte connexins. *Glia*. 59:26-34.
- Martinez, A.D., V. Hayrapetyan, A.P. Moreno, and E.C. Beyer. 2002. Connexin43 and connexin45 form heteromeric gap junction channels in which individual components determine permeability and regulation. *Circ Res*. 90:1100-1107.
- Martinez, A.D., J. Maripillan, R. Acuna, P.J. Minogue, V.M. Berthoud, and E.C. Beyer. 2011. Different domains are critical for oligomerization compatibility of different connexins. *Biochem J*. 436:35-43.
- Menichella, D.M., D.A. Goodenough, E. Sirkowski, S.S. Scherer, and D.L. Paul. 2003. Connexins are critical for normal myelination in the CNS. *J Neurosci*. 23:5963-5973.
- Menichella, D.M., M. Majdan, R. Awatramani, D.A. Goodenough, E. Sirkowski, S.S. Scherer, and D.L. Paul. 2006. Genetic and physiological evidence that oligodendrocyte gap junctions contribute to spatial buffering of potassium released during neuronal activity. *J Neurosci*. 26:10984-10991.
- Musil, L.S., and D.A. Goodenough. 1993. Multisubunit assembly of an integral plasma membrane channel protein, gap junction connexin43, occurs after exit from the ER. *Cell*. 74:1065-1077.
- Nagy, J.I., A.V. Ionescu, B.D. Lynn, and J.E. Rash. 2003. Coupling of astrocyte connexins Cx26, Cx30, Cx43 to oligodendrocyte Cx29, Cx32, Cx47: Implications from normal and connexin32 knockout mice. *Glia*. 44:205-218.
- Nakagawa, S., X.Q. Gong, S. Maeda, Y. Dong, Y. Misumi, T. Tsukihara, and D. Bai. 2011. Asparagine 175 of connexin32 is a critical residue for docking and forming functional heterotypic gap junction channels with connexin26. *J Biol Chem*. 286:19672-19681.
- Nelles, E., C. Butzler, D. Jung, A. Temme, H.D. Gabriel, U. Dahl, O. Traub, F. Stumpel, K. Jungermann, J. Zielasek, K.V. Toyka, R. Dermietzel, and K. Willecke. 1996. Defective propagation of signals generated by sympathetic nerve stimulation in the liver of connexin32-deficient mice. *Proceedings of the National Academy of Sciences of the United States of America*. 93:9565-9570.
- Odermatt, B., K. Wellershaus, A. Wallraff, G. Seifert, J. Degen, C. Euwens, B. Fuss, H. Bussow, K. Schilling, C. Steinhauser, and K. Willecke. 2003. Connexin 47 (Cx47)-deficient mice with enhanced green fluorescent protein reporter gene reveal predominant oligodendrocytic expression of Cx47 and display vacuolized myelin in the CNS. *J Neurosci*. 23:4549-4559.
- Orthmann-Murphy, J.L., C.K. Abrams, and S.S. Scherer. 2008. Gap junctions couple astrocytes and oligodendrocytes. *J Mol Neurosci*. 35:101-116.
- Orthmann-Murphy, J.L., A.D. Enriquez, C.K. Abrams, and S.S. Scherer. 2007a. Loss-of-function GJA12/Connexin47 mutations cause Pelizaeus-Merzbacher-like disease. *Mol Cell Neurosci*. 34:629-641.
- Orthmann-Murphy, J.L., M. Freidin, E. Fischer, S.S. Scherer, and C.K. Abrams. 2007b. Two distinct heterotypic channels mediate gap junction coupling between astrocyte and oligodendrocyte connexins. *J Neurosci*. 27:13949-13957.
- Orthmann-Murphy, J.L., E. Salsano, C.K. Abrams, A. Bizzi, G. Uziel, M.M. Freidin, E. Lamantea, M. Zeviani, S.S. Scherer, and D. Pareyson. 2009. Hereditary spastic paraplegia is a novel phenotype for GJA12/GJC2 mutations. *Brain*. 132:426-438.

- Paznekas, W.A., S.A. Boyadjiev, R.E. Shapiro, O. Daniels, B. Wollnik, C.E. Keegan, J.W. Innis, M.B. Dinulos, C. Christian, M.C. Hannibal, and E.W. Jabs. 2003. Connexin 43 (GJA1) mutations cause the pleiotropic phenotype of oculodentodigital dysplasia. *Am J Hum Genet.* 72:408-418.
- Paznekas, W.A., B. Karczeski, S. Vermeer, R.B. Lowry, M. Delatycki, F. Laurence, P.A. Koivisto, L. Van Maldergem, S.A. Boyadjiev, J.N. Bodurtha, and E.W. Jabs. 2009. GJA1 mutations, variants, and connexin 43 dysfunction as it relates to the oculodentodigital dysplasia phenotype. *Hum Mutat.* 30:724-733.
- Penes, M.C., X. Li, and J.I. Nagy. 2005. Expression of zonula occludens-1 (ZO-1) and the transcription factor ZO-1-associated nucleic acid-binding protein (ZONAB)-MsY3 in glial cells and colocalization at oligodendrocyte and astrocyte gap junctions in mouse brain. *The European journal of neuroscience.* 22:404-418.
- Rash, J.E., T. Yasumura, F.E. Dudek, and J.I. Nagy. 2001. Cell-specific expression of connexins and evidence of restricted gap junctional coupling between glial cells and between neurons. *J Neurosci.* 21:1983-2000.
- Saez, J.C., K.A. Schalper, M.A. Retamal, J.A. Orellana, K.F. Shoji, and M.V. Bennett. 2010. Cell membrane permeabilization via connexin hemichannels in living and dying cells. *Exp Cell Res.* 316:2377-2389.
- Salviati, L., E. Trevisson, M.C. Baldoin, I. Toldo, S. Sartori, M. Calderone, R. Tenconi, and A. Laverda. 2007. A novel deletion in the GJA12 gene causes Pelizaeus-Merzbacher-like disease. *Neurogenetics.* 8:57-60.
- Sartori, S., A.B. Burlina, L. Salviati, E. Trevisson, I. Toldo, A.M. Laverda, and A.P. Burlina. 2008. Increased level of N-acetylaspartylglutamate (NAAG) in the CSF of a patient with Pelizaeus-Merzbacher-like disease due to mutation in the GJA12 gene. *Eur J Paediatr Neurol.* 12:348-350.
- Scemes, E., and C. Giaume. 2006. Astrocyte calcium waves: what they are and what they do. *Glia.* 54:716-725.
- Scherer, S.S., Y.T. Xu, E. Nelles, K. Fischbeck, K. Willecke, and L.J. Bone. 1998. Connexin32-null mice develop demyelinating peripheral neuropathy. *Glia.* 24:8-20.
- Sohl, G., and K. Willecke. 2004. Gap junctions and the connexin protein family. *Cardiovasc Res.* 62:228-232.
- Stong, B.C., Q. Chang, S. Ahmad, and X. Lin. 2006. A novel mechanism for connexin 26 mutation linked deafness: cell death caused by leaky gap junction hemichannels. *Laryngoscope.* 116:2205-2210.
- Teubner, B., B. Odermatt, M. Guldenagel, G. Sohl, J. Degen, F. Bukauskas, J. Kronengold, V.K. Verselis, Y.T. Jung, C.A. Kozak, K. Schilling, and K. Willecke. 2001. Functional expression of the new gap junction gene connexin47 transcribed in mouse brain and spinal cord neurons. *J Neurosci.* 21:1117-1126.
- Tong, D., T.Y. Li, K.E. Naus, D. Bai, and G.M. Kidder. 2007. In vivo analysis of undocked connexin43 gap junction hemichannels in ovarian granulosa cells. *J Cell Sci.* 120:4016-4024.
- Tress, O., M. Maglione, A. Zlomuzica, D. May, N. Dicke, J. Degen, E. Dere, H. Kettenmann, D. Hartmann, and K. Willecke. 2011. Pathologic and phenotypic alterations in a mouse expressing a connexin47 missense mutation that causes Pelizaeus-Merzbacher-like disease in humans. *PLoS Genet.* 7:e1002146.

- Trexler, E.B., F.F. Bukauskas, J. Kronengold, T.A. Bargiello, and V.K. Verselis. 2000. The first extracellular loop domain is a major determinant of charge selectivity in connexin46 channels. *Biophys J.* 79:3036-3051.
- Uhlenberg, B., M. Schuelke, F. Ruschendorf, N. Ruf, A.M. Kaindl, M. Henneke, H. Thiele, G. Stoltenburg-Didinger, F. Aksu, H. Topaloglu, P. Nurnberg, C. Hubner, B. Weschke, and J. Gartner. 2004. Mutations in the gene encoding gap junction protein alpha 12 (connexin 46.6) cause Pelizaeus-Merzbacher-like disease. *Am J Hum Genet.* 75:251-260.
- Verselis, V.K., C.S. Ginter, and T.A. Bargiello. 1994. Opposite voltage gating polarities of two closely related connexins. *Nature.* 368:348-351.
- Volterra, A., and J. Meldolesi. 2005. Astrocytes, from brain glue to communication elements: the revolution continues. *Nat Rev Neurosci.* 6:626-640.
- Wang, J., H. Wang, Y. Wang, T. Chen, X. Wu, and Y. Jiang. 2010. Two novel gap junction protein alpha 12 gene mutations in two Chinese patients with Pelizaeus-Merzbacher-like disease. *Brain Dev.* 32:236-243.
- Wang, K.J., and S.Q. Zhu. 2012. A novel p.F206I mutation in Cx46 associated with autosomal dominant congenital cataract. *Molecular vision.* 18:968-973.
- Wang, W.H., Y.F. Liu, C.C. Su, M.C. Su, S.Y. Li, and J.J. Yang. 2011. A novel missense mutation in the connexin30 causes nonsyndromic hearing loss. *PloS one.* 6:e21473.
- Wasseff, S.K., and S.S. Scherer. 2011. Cx32 and Cx47 mediate oligodendrocyte:astrocyte and oligodendrocyte:oligodendrocyte gap junction coupling. *Neurobiol Dis.* 42:506-513.
- White, T.W., R. Bruzzone, S. Wolfram, D.L. Paul, and D.A. Goodenough. 1994. Selective interactions among the multiple connexin proteins expressed in the vertebrate lens: the second extracellular domain is a determinant of compatibility between connexins. *J Cell Biol.* 125:879-892.
- White, T.W., D.L. Paul, D.A. Goodenough, and R. Bruzzone. 1995. Functional analysis of selective interactions among rodent connexins. *Mol Biol Cell.* 6:459-470.
- Yamamoto, T., A. Ochalski, E.L. Hertzberg, and J.I. Nagy. 1990. LM and EM immunolocalization of the gap junctional protein connexin 43 in rat brain. *Brain Res.* 508:313-319.

Curriculum Vitae

Mi Seong Kim

OBJECTIVE:

To broaden knowledge and gain meaningful experience in scientific research in the field of physiology

EDUCATION:

2010 - 2012 M.Sc Physiology, Class of 2012
University of Western Ontario, London, ON.

2006 - 2010 B. MSc Honours Specialization in Physiology.
University of Western Ontario, London, ON

AWARDS & ACCOMPLISHMETNS:

2010-2011 Ontario graduate scholarship grant (3 terms)
University of Western Ontario, London, ON.

2011 UWO Physiology & Pharmacology Research Day (poster presentation)
University of Western Ontario, London, ON.

2010 UWO Physiology & Pharmacology Research Day (poster presentation)
University of Western Ontario, London, ON.

2006-2010 Dean's List
University of Western Ontario, London, ON.

2006 Western University entrance scholarship
University of Western Ontario, London, ON.

EMPLOYMENT:

2010-2012 University of Western Ontario, London, ON
Graduate teaching assistant

2009 University of Western Ontario, London, ON
Research assistant